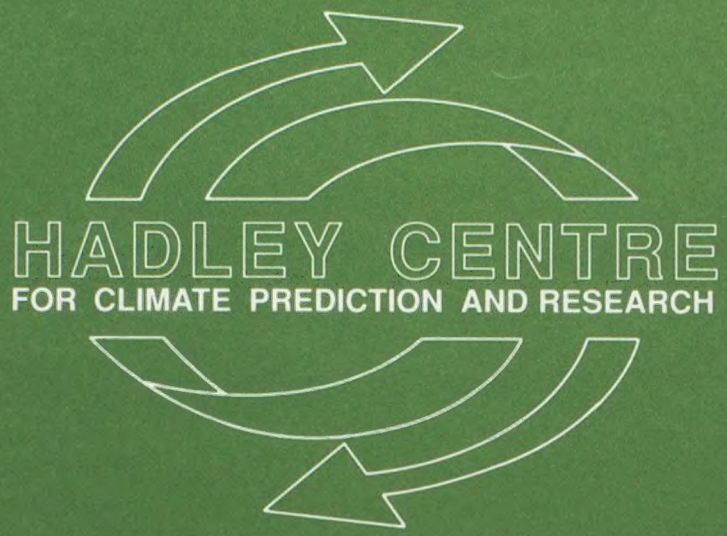

Large scale modes of ocean surface temperature since the late nineteenth century

by

C K Folland, D E Parker, A W Colman
and R Washington

CRTN 81

February 1998

CLIMATE
RESEARCH
TECHNICAL
NOTE

Hadley Centre
Meteorological Office
London Road
Bracknell
Berkshire RG12 2SY

Large scale modes of ocean surface temperature since the late nineteenth century

C K Folland*, D E Parker*, A W Colman* and R Washington+

*Hadley Centre, Meteorological Office, Bracknell, U.K.
+School of Geography, University of Oxford, U.K.

Abstract

We investigate multi-decadal variability in observed ocean surface temperatures and in rainfall since the late nineteenth century, with emphasis on quasi-bidecadal variability. This is carried out against a background of large scale ocean surface temperature variations on the shorter time scales of the El Nino-Southern Oscillation (ENSO). On multi decadal time scales, a quasi-El Nino pattern is seen in the sea surface temperature (SST) that extends further west into the tropical West Pacific than on ENSO time scales. It has broadly similar relationships to tropical rainfall as seen on interannual time scales. A fairly striking relationship between Southern African rainfall and large scale SST patterns since 1900 is shown for quasi-bidecadal and longer time scales.

1. Introduction

There is increasing evidence of coherent patterns of variability on near quasi-bidecadal time scales in a range of climatic data from many parts of the world. Folland et al. (1984) found peaks at periods of 16 and 21 years respectively in spectra of globally-averaged sea surface temperature (SST) and night marine air temperature (NMAT) for 1856-1981. Newell et al. (1989) found variations near a period of 21 years in global and Southern Hemisphere NMAT for 1856-1986, and to a lesser extent in Northern Hemisphere NMAT and global and hemispheric SST. Ghil and Vautard (1991) drew attention to variations on approximately 20-year time-scales in globally-averaged anomalies of combined land surface air temperature and SST for 1854-1988, though Allen and Smith (1996) question the statistical significance of their results. Mann and Park (1994) found a 15-18 year mode in fields of mainly land surface air temperature anomalies for 1891-1990. They suggested that this mode, which had a pattern similar to that of the thermal signature of the interannual El Niño-Southern Oscillation (ENSO), may be a manifestation of long timescale modulation of ENSO as well as being the reason for Ghil and Vautard's (1991) global-average result. Latif and Barnett (1996) discussed near bidecadal variations in SST and atmospheric circulation over the North Pacific in both observations and a coupled model, and the consequential variations of temperature and precipitation over North America. In the Southern Hemisphere, Venegas et al. (1996) found a coupled mode in South Atlantic SST and mean sea level pressure (MSLP) data for 1953-1992, with significant variations on near 15-year timescales and provided evidence that the atmosphere was forcing the ocean. The fluctuations of this mode were significantly correlated with those of the interdecadal joint mode of Northern Hemisphere surface temperature and MSLP found by Mann and Park (1996). Chang et al. (1997) found a 13-year spectral peak in their analysis of a dipole of SST anomalies straddling the equator in the Atlantic, a result close to that of previous authors. The dipole was strengthened by a positive feedback with wind-

induced heat fluxes, and damped by ocean currents. However, they found no close relationship with the leading global-scale mode of SST. In addition, New Zealand land air temperatures were compared with nearby SST and NMAT by Folland and Salinger (1995). New Zealand Temperature (NZT) for 1871-1993 displayed prominent one to two decade variations peaking near a period of 16 years, which were well replicated in neighbouring (30^0-50^0S, 165^0-180^0E) SST and NMAT data. However these variations were only marginally coherent with SST variations on quasi-bidecadal time-scales in the tropical Eastern Pacific or variations averaged over the Southern Hemisphere as a whole. Note that 14-18 years is a shorter period than the 21-year peak noted by Folland et (1984) or Newell et al. (1989). In tropical East Pacific SST there is a near 14-15 year peak (Figs 2n,o), though a peak near 20-30 years is more prominent in NMAT.

Particularly relevant results have been shown by Zhang et al. (1997) and Mantua et al. (1997). Zhang et al. identify a decadal to multi decadal ENSO-like mode of sea surface temperature which has a distinctly different pattern in the east Pacific compared to the normal ENSO pattern and has more variability in the North west Pacific than does ENSO. Mantua et al. call a similar pattern the "Pacific Decadal Oscillation". We refer to these results later.

In this chapter we attempt to isolate the regions contributing most strongly to near bidecadal variability against the background of variations on El Nino-Southern Oscillation to century time scales. We demonstrate connections between ocean surface temperatures and tropical rainfall patterns on near bidecadal time-scales, and compare these relationships with already-established links with ENSO on interannual time-scales. Particularly strong links appear between southern African rainfall and SST anomalies.

2. Data

Our main marine surface temperature data are SSTs from the Meteorological Office Historical Sea Surface Temperature (MOHSST6C) data set (Parker et al., 1995c). They are expressed as monthly anomalies on a 5^0 latitude x 5^0 longitude resolution from the 1961-1990 climatology of Parker et al. (1995b) and Rayner et al. (1996) and include the bias adjustments to pre-1942 SST data in Folland and Parker (1995). Missing monthly values with at least four spatially or two temporally adjacent neighbours are replaced by the average of these neighbours, as described by Parker et al. (1994). Outlying values, defined as deviating by more than 2.25^0C from the average of these neighbours, are likewise replaced (*op. cit.*). As supporting evidence, we use NMAT anomalies relative to 1961-90 from the recent Meteorological Office Historical Night Marine Air Temperature (MOHMAT42) data set (updated from Parker et al., 1995a). Bias-adjustments, smaller than those applied to SST, are also applied to older NMAT (Parker et al., 1995a).

The Global Sea Ice and Sea Surface Temperature Data Set (GISST) was not used. Earlier versions (Parker et al, 1995a) relax some regions to climatology. Later, better versions (Rayner et al., 1996) use eigenvector reconstruction methods which would impose some of the patterns investigated here. However, as described in Appendix 1, we have adapted a step used in Rayner et al. (1996) to create the eigenvector time series calculated in Section 3.4. This "enhancement" method gives almost unbiased estimates of the variance when marine data are incomplete. It boosts the variance of

ENSO dominated EOF time series, particularly before 1950, in a similar way to that which occurs in the full GISST2 data.

Gridded precipitation data are updated from Hulme (1994). The southern African regional rainfall series used in Section 5 was derived from these data as follows. Gridded monthly values, at 2.5° latitude x 3.75° longitude resolution, were converted into seasonal anomalies for January-March, using 1951-1980 as the reference period. The anomalies were passed through a Kalman low-pass filter (Young et al., 1991) with half-power at a period of 13.3 years to remove ENSO-related variability and to concentrate on the near bidecadal time scale and its longer term modulation. Unrotated correlation empirical orthogonal functions (EOFs) of Africa-wide rainfall (south of 25°N) were then calculated. The first EOF has large weights of one sign over southern Africa, including South Africa, Namibia, Lesotho, Swaziland, Botswana, Zimbabwe and extreme southern Mozambique. The corresponding time series correlates (r=0.90, significant at the 95% level) highly with an areal average of filtered rainfall over the broad southern African region. This time series was used as the 'observed' rainfall series in Section 5.

3. Low frequency variability in marine surface temperatures

3.1. Global and regional time series of SST and NMAT anomalies

Figure 1 shows global, hemispheric, and a selection of regional seasonal time series of SST (MOHSST6C) and NMAT anomalies for 1861-1996. Low-pass filtered series are superimposed using the method described in Section 2. These are much like the series shown in Bottomley et al. (1990). Bidecadal variability is particularly evident between 1870 and 1950 in the South Pacific but is less evident in the North Pacific. We choose to show marine data for the South Atlantic averaged over 0°-20°S in Fig. 1e because it best demonstrates the quasi-15-year fluctuation found by Venegas et al. (1996). It is especially evident after 1970 (in accord with the their findings and those of Chang et al. 1997), but also appears between 1890 and 1940. All the series in Fig. 1, especially those for the smaller regions, show reduced inter-seasonal coherence in the nineteenth century, and especially prior to 1875, when data were very sparse, as noted by Bottomley et al. (1990). Note the often high level of agreement between the SST and NMAT data down to the seasonal time scale in recent decades, with few exceptions.

3.2. Power spectra

Complete annual time-series of temperature anomalies were required to estimate power spectra. For the globe, hemispheres and ocean basins, the marine data yield complete annual series: for the smaller regions, Nino 1+2 area, (0°-10°S, 80°-90°W) and Nino 3.4 area (5°N-5°S, 120°-170°W) linear interpolation was used.

Figure 2 shows power spectra of detrended annual SST (thick lines) and NMAT anomalies (thin lines) for the globe, hemispheres and a range of regions. (The spectra are based on the fourier transform of the autocorrelation function of detrended data, using about one third as many autocorrelations as data). The spectra are for 1876-1996 except for the west tropical Pacific and the Nino 1+2 area where the periods are 1898-1996 and 1906-1996 respectively. The 95% estimates of significance use a

method due to Allen and Smith (1996) that allows for coloured noise as an AR(1) process. Values of power significant at the 95% confidence level criteria are often very high because of the strong annual autocorrelation in many series; thus r_1=0.70 for the Northern Hemisphere. Consequently few low frequency spectral estimates are significant. This problem is related to the short length of the historical record so that we cannot adequately distinguish between multidecadal variability that is part of an AR(1) process and variability resulting from processes in a particular frequency band. Where NMAT and SST spectra differ at periods beyond several decades, the SST spectral estimates are more reliable.

Many series show peaks near the main ENSO time scales of around 3.5-6 years that dominate the spectra for NINO3.4 and Nino 1+2 (Figs 2n and 2o), (Rasmusson and Carpenter, 1982). The globe, Southern Hemisphere and Northern Hemisphere all show significant peaks near a period of 4 years, as do many Southern Hemisphere ocean regions (e.g. Figs 2f, g, p). Some regions like the South Pacific show muted power because large warm and cold sub-regions associated with ENSO are prominent at the same time. The general warming and cooling of the Indian Ocean associated with ENSO shows up in Figs 2i and 2m as peaks with periods near 3.5-5 years.

On longer time scales, quasi- bidecadal variations are evident, weakly for the globe but more strongly in the Southern Hemisphere (Figs 2a,e,f), in accord with Folland et al. (1984), though the peaks are not significant. Interestingly the NMAT peaks are stronger, though NMAT data are less reliable than SST data. Century-scale variations are more dominant in both data sets, though even these are not significant. In the Northern Hemisphere (Fig. 2b), there is *minimum* power at 15-20 years in SST with a very weak maximum near 10 years. There is no bidecadal peak in the *annual average* SST of three main Northern Hemisphere oceans (Figs 2c,d and l) though weak near decadal peaks are evident, but these are not statistically significant. The North Atlantic variations seen on near 10-year time scales appear to originate more from the tropics (0^0-20^0N, see also Chang et al., 1997) than from higher latitudes (>35^0N, not shown). Although most of the latter area has similar phase in the decadal dipole found by Deser and Blackmon (1993), their result was based on winter data, so our findings based on annual data may not contradict theirs. The North Atlantic also shows the largest variation on a sub-century time scale. The western tropical Pacific (20^0N-20^0S, 120^0E-170^0W, Fig. 2k) also shows near 10-year variations which almost reach 95% significance level for NMAT. In the Southern Hemisphere, a peak corresponding to bidecadal variations is strongest and nearly significant in the South Pacific in NMAT (Fig. 2h), but weaker in the southern Indian Ocean (Fig. 2m) and southern tropics (Fig. 2p), and not evident in the tropical South Atlantic (Fig. 2g). By contrast, in the tropical South Atlantic 12-14 year variations corresponding to those found by Venegas et al. (1996) and Chang et al. (1997) are prominent and just statistically significant for NMAT; similar results are found when the domain is extended to 30^0S (not shown). There are no important spectral peaks near 20 years in the warm pool area 15^0N-10^0S, 65^0-180^0E (Fig. 2j), though SST has the hint of a peak near 15 years, or in the western tropical Pacific (Fig. 2k). In the Nino 1+2 area 0^0-10^0S, 80^0W-90^0W (Fig. 2o), there are non-significant multi decadal variations in NMAT, but not in SST: there is a weak peak near 14 years in both. The Nino 3.4 area, 5^0N-5^0S, 120^0-170^0W, shows statistically insignificant but moderately prominent 12-14 year variations and bidecadal variations around 25 years especially in NMAT. These are (Fig. 2n) weaker, as expected, than 4-6 year variations associated with El Niño, though the NMAT variation is not much

weaker Fig. 2n highlights the limitations of the estimates of statistical significance: even the well known longer time scale ENSO fluctuations around 5-7 years are significant.

We now investigate spatial patterns of near bidecadal variability in annual data.

3.3. Spatial patterns of near bidecadal ocean surface temperature variability

To estimate these patterns, we calculated global fields of low-frequency (LF) filtered SST and NMAT. First, seasonal (January-March etc.) mean anomalies for almost equal-area grid boxes (of dimension 10^0 latitude x 12^0 longitude at the equator) were formed by averaging all available monthly anomalies for 5^0 latitude x 5^0 longitude areas that contributed to the equal-area box. Anomalies for these 5^0x5^0 boxes were weighted according to the proportion of area covered within the equal-area box. An equal area box was used if there were at least 144 (40%) of seasons available between 1901 and 1990. Seasonal anomalies for equal area boxes were set to missing if there were fewer than 10 monthly anomalies available from their constituent 5^0x5^0 boxes. This criterion allows early, sparser, data to contribute as much to the analysis as possible without compromising its quality. Temporally complete LF data were then calculated using a Kalman low-pass filter with half-power at a period of 13.3 years. This time scale not only eliminates the usual ENSO time scales but it was also chosen to remove the near decadal time scales prominent in the North and tropical Atlantic which are beyond the scope of this study.

Fig 3a depicts the standard deviation of LF annual SST anomalies for the epoch 1911-1995 falling in the "near bidecadal" (18-30 years) range of periods, and Fig 3b the standard deviation as a percentage of the standard deviation at all periods > 13 years. Figs 3c,d are corresponding maps for the (slightly overlapping) "sub-bidecadal" 13-18 year range seen more in New Zealand surface air temperature.

Fig 3a shows the highest values of 18-30 year standard deviation in the central Pacific from south of Alaska to at least 50^0S with maximum (reliable) standard deviations of SST just south of the equator around 120°-140°W. Values reach 0.2° C in the latter region, twice the mean global standard deviation of 0.1°C. Expressed as a percentage of local standard deviation on LF time scales >13 years, peak values are almost in the same region but extend south west to 160°W, 20°S, exceeding 60% around 15° S, 150°W. An area exceeding 55% occurs in the tropical eastern-most Pacific. Note that relatively large percentages extend across much of the tropical Pacific. In other oceans the maximum standard deviations are less and percentages only reach about 45% except perhaps for a small region in the Gulf of Guinea. The near decadal variability prominent in the tropical Atlantic is highly attenuated at these periods.

Fig. 3c shows a fairly similar picture for the 13-18 year time scale but with lower standard deviations (global mean 0.09°C). Expressed as a percentage of the total LF standard deviation (Fig. 3d) the peak values of >50% are less concentrated but still tend to extend across the tropical Pacific. Percentages near New Zealand are higher than for the 18-30 year interval but only reach 35-40% so it appears that the seat of the New Zealand 14-18 year temperature variations (presumably reflected in atmospheric circulation variations too) may lie over the tropical Pacific. The very large peak in absolute (Fig. 3c) and percentage standard deviation near 150°W, 50°S should be

noted but requires the GISST data set for further analysis. This is a higher latitude region identified tentatively by Folland and Salinger (1995), and more definitely by Folland et al. (1997) using GISST2 as being quite strongly influenced by ENSO probably via a systematic modulation of the strength of the westerly winds.

3.4. Synthesis of variability: Empirical Orthogonal Function (EOF) analysis

We calculated LF global unrotated covariance all-seasons EOFs from the LF marine data and a corresponding set of high frequency (HF) EOFs (periods <13 years), all for 1911-1995. Many authors have calculated global SST EOFs, mostly over shorter periods e.g. recently Kawamura (1994). Our EOFs update those of Parker and Folland (1991) who did not distinguish between the HF and LF time scales and we use the EOF time series enhancement technique described in Appendix 1. Note that choice of the the boundary of the LF time scale at 13.3 years (half power at this period) is not only compatible with the Southern African rainfall analyses but is deliberately designed to suppress near decadal variations prominent in the Atlantic which may confound the lower frequency LF results shown below. Interpolated values were *excluded* from fields input to the EOF analyses. We also excluded some coastal and landlocked sea areas in middle and high latitudes of the Northern Hemisphere, because the high variance of anomalies in these areas was found to have a disproportionate effect on the shape of the leading global EOFs. We chose covariance EOFs to highlight areas of strong absolute low frequency variability.

Figure 4 depicts the first four LF EOFs of SST for 1911-1995 (Fig. 4a,d,f,i), along with their enhanced time series (Fig. 4c,e,g and j). LF EOF1 (45.5% of LF variance, 10.3% of total all-seasons variance) is of one sign over almost all the domain, and represents global century-scale trends, much as shown by Parker and Folland (1991). LF EOF1 is very similar to the corresponding field of linear SST trends for 1911-1995 (Fig. 4b), with a field correlation of 0.93. Thus the pattern of LF EOF1 represents the *regional detail* of global temperature trends from the full data set very well so we contend it is an excellent representation of the main pattern of global warming in SST this century. Thus it picks up the lack of warming south of Greenland though not the full extent of recent cooling there (Fig 4b). The time series of LF EOF 1 has a correlation of 0.97 with the LF global-average SST anomaly over the extended period 1861-1996 (Fig. 4c) so it is likely to represent the chief pattern of global marine temperature change in the late nineteenth century as well. The second LF EOF (15.3% of LF variance, 3.4% of total all seasons variance) represents the interhemispheric contrast associated by Folland et al. (1986), Parker and Folland (1991) and Folland et al. (1991) with decadal episodes of Sahel wetness or drought. LF EOF2 contributes considerably to the multi decadal SST changes in the North Atlantic linked by Kushnir (1994) to regional atmospheric circulation changes. Its time series suggests variation on time scales of about 60-70 years. LF EOF2 is likely to be a manifestation of variations in the thermohaline circulation and temperature on the same time scale described by Schlesinger and Ramankutty (1994).

LF SST EOF3 (12.7% of LF variance, 2.9% of total variance, Fig. 4f) appears to be the focus of some bidecadal SST variability (Fig. 4g), though lower frequency variations dominate its spectrum (Fig. 4h). LF EOF3 has a pattern somewhat reminiscent of ENSO related SST patterns (see Fig 6a). However it is not the same; the weights over the North west Pacific exceed in magnitude those of opposite sign over the tropical east

Pacific. Nevertheless, the Indian Ocean, like ENSO, has weaker weights than in the tropical East Pacific but of the same sign. Another difference is the near zero weights over the easternmost Tropical Pacific. This helps to give the impression of an almost "horseshoe" shape of positive weights stretching from California through the equator to 15°S, 90°W seen also by Latif et al. (1997) in an LF principal oscillation pattern analysis and by Kleeman et al. (1996) for the "extended ENSO" period of 1990-1994 (their Fig. 1a). In the South Pacific again the pattern is like that associated with ENSO but the negative weights are relatively larger in magnitude than in Fig. 6a. Over the Atlantic the weights are small and positive and possibly not reliable. Recently Kachi and Nitta (1997) also show a broadly similar mode (their Fig. 9) using a singular value decomposition analysis. They analyse decadal variations in (I) December to February SST for 60°N to 40°S and (ii) decadal variations in 500hPa height over the Northern Hemisphere , both from 1955 to 1995. The relative lack of variance over eastern most Pacific SSTs is again seen and many other SST features are fairly similar to our LF EOF3. Another less certain feature of our analysis is the extension of positive weights across the tropical West Pacific, again not seen on ENSO time scales. LF SST EOF3 is quite similar to LF SST EOF2 of an earlier unpublished analysis by Folland et al. (1993). The spectrum of LF SST EOF3 (Fig 4h) shows a modest peak around 30 years.

The main features of LF SST EOF3 in the Pacific are borne out by LF NMAT EOF3 (Fig. 5a). Although the Indian Ocean centre is weaker in the NMAT analysis and the Atlantic has low weights of mixed sign, the correlation between the fields in Figs 4f and 5a is 0.70, and the correlation between the time series in Figs 4g and 5b is 0.77 over 1861-1996. Interestingly, the patterns in Figs 4f and 5a, and the associated time series, seem consistent with the low frequency variations in Aleutian region winter mean sea level pressure and its relationships with surface temperature discussed by Trenberth and Hurrell (1994).

LF EOF3 is similar to the "Pacific Decadal Oscillation" of Mantua et al. (1997) and particularly to the first global EOF of unfiltered SST of Zhang et al. (1997). Zhang et al eliminated the effect of global warming by calculating an adjusted SST anomaly data set (based on MOHSST) expressed as the difference of their anomalies from the global mean SST anomaly for the current year. They call such quantities "anomaly deviations". They carried out this procedure because they considered that forcing the remaining global EOFs to be orthogonal to a "global warming" EOF (our LF EOF1) was too strong a constraint. We appear to overcome this problem by filtering SST into separate LF and HF time scales. However Zhang et al. do not report our EOF2, though their analysis concentrates on ENSO-like patterns and they also use a smaller global domain (60°N-30°S). We consider the Zhang et al. "global" SST pattern (and their even more similar comparable SST pattern for 1950-93) is close to our LF EOF3 for 1911-1995. Thus the time series in our Fig. 4g is quite like (but smoother than) the six year low pass filtered time series of their "global pattern" over this century. Our analysis method and results differ from theirs in several other respects. So this highlights the problem of the most incisive, or most parsimonious, methodology for studying large scale SST patterns.

Global LF SST EOF4 (Fig. 4i, 6.6% of LF variance, 1.6% of total variance) is included because of its quite strong relationship to LF southern African rainfall in Section 5, though we do not claim this pattern is as "real" globally as that of the first three LF SST EOFs. EOF4 has weights concentrated in the central Pacific, and weights of opposite

sign in the north west Atlantic and South Indian Ocean. The time series shows a minimum around 1935-1950 and a maximum in the 1960s. Its spectrum (Fig 4k) shows comparable power across the resolvable low frequency spectrum.

The first 4 LF SST EOFs explain as much as 80.1% of the total LF variance over 1911-1995, and 18.0% of all variance. Although a little bidecadal variability is evident in the higher order LF EOFs, a fuller study requires rotation of the EOFs to localize the patterns, and is beyond the scope of this paper.

Figure 6 shows the first two HF EOFs (a,b) and their enhanced time series (c). HF EOF1 (12.6% of total variance, Fig. 6a) represents the usual picture of the mature phase of ENSO warm events, while HF EOF2 (3.5% of total variance, Fig. 6b) has negative weights in the tropical eastern-most Pacific but positive weights in the central Pacific and greater relative weight in the Indian Ocean than HF EOF1. HF EOF2 is lag-correlated with HF EOF1 (Fig 6d) and tends to peak (with the same sign) about 2-3 seasons (six-nine months) later (Fig. 6c,d). Presumably it tends to reflect the more muted pattern of the transition between El Nino and La Nina or La Nina and El Nino but clearly not always (Fig 6c). Thus the 1982-83 El Nino showed almost no projection onto HF EOF2. The extended 1991-1995 El Nino conditions projected clearly onto HF EOF1 but only late 1990 and mid 1995 projected onto HF EOF2. The peak correlation at two seasons lag of 0.56 between HF EOF1 and HF EOF2 in Fig. 6d is highly significant. It is consistent with greater relative positive weights in the Indian Ocean in HF EOF2 as Indian Ocean warming tends to lag Tropical East Pacific warming by one to two seasons but it is less clear whether the marked positive weights in the tropical Atlantic are real. This would imply a tendency for appreciable warming in this region two or three seasons after the peaks of at least some ENSOs.

We have calculated the squared coherence between the seasonal time series of the LF SST EOF3 and the normalized unfiltered seasonal Tahiti minus Darwin mean sea level pressure Southern Oscillation Index (SOI, Ropelewski and Jones, 1987), for 1871-1995 (not shown). The squared coherence peaks at 0.47, marginally significant at the 95% level, at a period of 20 years. For LF NMAT EOF3, coherence squared peaks at 0.72, strongly significant at a period of 24 years. This suggest that the LF EOF 3 pattern imposes a "bidecadal" (20-30 year) signal on, or receives one from, atmospheric circulation variations measured by the Southern Oscillation index. The stronger coherence with NMAT requires further investigation but note that LF NMAT EOF3 has relatively more weight in the tropics between 150°-180°E.

3.5 Extended EOF analysis of LF SST

We have carried out an extended EOF analysis of the LF SST data to determine whether seasonal variability of the LF SST EOF patterns is likely to be important. Table 1 shows correlations between the spatial weights of the LF all seasons EOFS and the LF EEOFS for each season for EEOFs 1-4. LF EEOFs 1-4 all explain similar amounts of variance to the corresponding all seasons LF EOFs. We have used the "year" April to March to optimise the consistency of corresponding HF EEOFS (not discussed here) where we try to avoid the frequent transition from El Nino to La Nina or the reverse around April. The correlations are generally high, and in fact remarkably high for EOF4 and the corresponding seasonal EEOFS which suggests that LF EOF4 may after all reflect a "real" quasi-global pattern. Table 1 indicates all listed seasonal EEOFs are

essentially the same as the corresponding all seasons EOFs. Beyond EOF4 (not shown) correlations suddenly drop. The lowest correlations in Table 1 are between LF EOF3 and its corresponding seasonal EEOFs. Figs 6a-d show the four seasonal EEOFs. They are all quite similar to each other and to LF EOF3 (Fig. 4f). Scrutiny of Fig 6a, least similar of these diagrams to Fig 4f (correlation 0.57), shows detailed differences in the patterns of local weights, and regionally in the position of the zero line, but the overall large scale pattern is surprisingly similar. We conclude that the seasonal patterns are sufficiently similar allowing for sampling error that further analyses can concentrate on the all seasons SST LF EOFS1 to 4. This agrees with the result obtained by Graham (1994); he found an SST pattern in NH winter very like the tropical part of LF EOF3 between 20°N and 20°S, 110°E to 70°W, when he subtracted 1977-1982 winter SST from that of the colder period 1971-76.

TABLE 1 CORRELATIONS BETWEEN SPATIAL WEIGHTS OF LF SST EOFS AND LF SEASONAL SST EEOFS, 1911-1995 OR 1912-1996 FOR JANUARY TO MARCH.

ALL SEASONS SST EOF	JAN-MAR LF EEOF	APR-JUNE LF EEOF	JULY-SEPT LF EEOF	OCT-DEC LF EEOF
LF EOF 1	0.87	0.77	0.82	0.83
LF EOF 2	0.71	0.74	0.81	0.77
LF EOF3	0.80	0.57	0.80	0.76
LF EOF4	0.82	0.82	0.82	0.83

3.6 Stability of the all seasons EOF analyses.

All seasons EOFs were recalculated for the period 1901-1990. These had an increased tendency to similarity of eigenvalues and mixing of some leading modes. This is expected when the input data are geographically sparse (Kim, 1996), as was true for the Pacific at the beginning of the century. We also repeated the SST EOF analyses for 1921-1955 and 1956-1990 (not shown). The period 1921-1955 was chosen because it covered the epoch of weakened conventional ENSO relationships (Allan at al., 1996) whereas these connections were stronger in 1956-1990. However, in the LF analysis for 1921-1955, only EOF1 retained its integrity: higher modes were not resolved well by the short record. In the LF analysis for 1956-1990, even EOFs 1 and 2 were mixed. This result indicates that some of the patterns of interdecadal variability can be identified with about a century of data, but a full identification cannot be made. However, valuable insights can be gained through diagnosis of the processes at work through one or two cycles (e.g. Kleeman et al., 1996). A further general concern is that the weights of LF EOF2 and to a slightly lesser extent, EOF3, are large over many data sparse regions; this includes the tropical and South Pacific and other southern extratropical oceans. These caveats should be borne in mind in the remainder of the paper. On the other hand, HF SST EOF1 was well preserved in both periods, and HF EOF2 was also similar to 1911-1995 in the Pacific and Indian Ocean, but in the 1921-1955 analysis there were differences in the tropical Atlantic where, as noted above, the

rather strong weights in 1911-1995 need confirmation.

We also repeated the all seasons SST EOF analyses for 1911-1995 with the domain restricted to the Pacific. Because LF global EOF3 is largely a Pacific mode (Fig. 4f), the corresponding mode in the Pacific-only analysis was very similar (not shown) but became EOF2 for that ocean, explaining 17.2% of its LF variance, as against 12.7% of the global LF variance for LF SST EOF3.

4. Relationships between marine surface temperatures and tropic-wide rainfall on multi decadal time-scales.

We found above that LF EOF3 had a pattern quite like HF EOF1 in many respects. To determine if and how LF EOF3 influences LF rainfall, correlations were calculated between the time series of LF global SST EOF3 (Fig. 4g) and gridded LF seasonal worldwide (land only) rainfall for 1901-1995 for January-March and July-September. The tropical and subtropical (40°N-40°S) parts of these correlation patterns are shown in Figs 8a and 8b respectively. For comparison, we calculated EOF1 of *unfiltered* rainfall for 20°N-40°S in January-March and EOF1 of unfiltered rainfall for 40°N-20°S in July-September over the same period (Figs 9a,d). The strong link of the former with ENSO is shown in Fig. 9b where the seasonal time series of HF SST EOF1 (which represents the mature phase of ENSO most typically around January) has a simultaneous correlation of 0.80 with the time series of January-March rainfall EOF1. Both time series were enhanced as described in Appendix 1. The correlation in July-September is lower at 0.70 (Fig 9e). Most interestingly, the two unfiltered rainfall EOF1s have pattern correlations of 0.61 and 0.46 respectively with the fields of Figs 8a and 8b over 1901-1995. Thus moderately similar relationships between SST and rainfall with an ENSO-like global tropical pattern exist on both HF and LF time scales

The patterns in Figs 8b and 9d, particularly the weights of the same sign from India to the Caribbean are reminiscent of a boreal summer tropic-wide mode of precipitation found by Ward et al. (1994). Similar patterns are also found by correlating gridded rainfall with the time series of the equivalent LF Pacific-only SST EOF 2 (Section 3.4) or with the unfiltered SOI (not shown). Graham estimated the differences in rainfall in NH winter between 1977-82 and 1971-76 for the tropical Pacific. Graham's Fig. 4c is consistent with the implied pattern of rainfall differences between warmer and colder tropical Pacific phases of LF EOF3 shown in the same area of Fig 8a. However we lack rainfall data in the tropical East Pacific east of 130°W; here Graham showed an increase of rainfall just north of the equator and a decrease just to its south. Nitta and Kachi (1994) have carried out analyses of decadal changes in annual rainfall in the tropical Pacific and related these to decadal changes of SST since 1955. Their annual results are not strictly comparable with our seasonal analysis but their finding of increased rainfall in the central tropical Pacific since the mid 1970s again agrees well with our Figs 8 and 9.

Figs 9c and 9f show power spectra associated with the unfiltered rainfall EOFs in Figs 9a and b. Both spectra show some quasi-bidecadal variability more evident in January-March, though the bidecadal power is not statistically significant. This implies that some Southern Hemisphere tropical regions with rainfall maxima in this season are particularly likely to experience bidecadal modulation, perhaps those with larger weights in Fig. 9a and 9d. We now investigate LF southern African rainfall where strong

negative weights can be seen in Fig 9a. As explained in Section 2, LF southern African rainfall is represented by its first EOF.

5. Low Frequency relationships between marine surface temperatures and southern African rainfall.

The importance of the quasi-bidecadal component of southern African rainfall has long been known (Tyson, et al., 1975) and is perhaps the best studied rainfall variation on this time scale. Although near bidecadal variability explains less than 30% of the total rainfall variability, the underlying oscillation has been used to predict the prolonged southern African drought of the 1980s (Tyson and Dyer, 1980), and to infer the climates of the Last Glacial Maximum (Cockcroft et al., 1987), the late Holocene (Tyson and Lindesay, 1992; Cohen and Tyson, 1995) and the next century (Tyson 1991). Physical mechanisms to explain this variability have, however, remained elusive.

Figure 10a shows the time series of LF southern African January-March rainfall (1900-1991) by the solid line. It shows strong variability on the quasi-bidecadal time scale (22 years is sometimes claimed but this is too precise) with a major peak around 1910, a minor peak around 1935, and major peaks near 1950 and 1975.

Table 2 Multiple Regression Statistics of Southern African Rainfall and SST EOFs

STEP	LF SST EOF	F	R^2
1	EOF4	48.81	0.35
2	EOF3	77.94	0.64
3	EOF2	116.66	0.80

Table 2 shows stepwise multiple regression statistics for LF SST EOFS 2-4. F is the F ratio significance statistic and R^2 the coefficient of determination for each step. The best fitting individual EOF is LF EOF4 with a correlation of 0.59. The southern African droughts of the 1980s, 1960s and 1920s, together with the wet spells of the 1970s and 1950s, are in phase with the modulation of SST by LF EOF4. A plot of LF EOF4 against the rainfall (not shown) indicates that EOF4 simulates the rainfall variability well except between 1935 and 1950 when it grossly overpredicts the amount. Addition of EOF3 largely corrects this and the further addition of EOF2 which varies on a time scale near 60 years improves the overall fit to give a correlation of 0.89. The dashed line in Fig 10a shows the simulated Southern African rainfall based on these three LF SST EOFs. We judge these three LF SST EOFs to add statistically significant variance at the 95% confidence level according to the F ratio, based on estimates of the number of degrees of freedom in the LF time series calculated from their serial correlations. These three EOFs explain 34.6% of the LF SST variance in 1911-1995. Note that LF SST EOF1, global climate change, explains no significant rainfall variance even though it explains more LF SST variance (45.5%) than the three explanatory EOFS put together.

We do not show maps of the local correlations of LF SST and Southern African rainfall because a provisional analysis indicates some strong temporal variations. Thus strong correlations exist with the Tropical East Pacific in 1900-1925 and 1956-1991 but in the

intermediate 30 years (1926-1955) these correlations are weak. The strongest correlations then occur with LF SST around 10-20°S, 120°W. Our EOF representation has somehow picked up these changes to a considerable extent. This needs more investigation. However we feel it useful to give an indication of the SST differences that are involved between wet and dry conditions. The absolute values of SST vary strongly through the century because of climate warming, affecting both wet and dry values in a broadly similar way and this can be aliased onto a small sample of extreme years sampled in LF mode. So Fig. 10b shows the differences in *linearly detrended* SST between the wettest 25% of LF Southern African rainfall values and the driest 25% of values. Detrending the rainfall makes little difference to the pattern. The regression equation will of course allow a variety of patterns to correspond to a given LF rainfall percentile depending on the relative strength of the constituent EOF time coefficients. Fig. 10 shows a broadly El Nino-like pattern but with only small differences in SST near the South American coast consistent with the pattern of, and strong effect of, LF EOF3. The largest differences in SST are displaced into the northern tropical Pacific around 160°W consistent with EOF4. Tests of the regression equation for 1900-1991 suggests that it places more weight on SST differences (of the same sign) south east of South Africa than indicated in Fig. 10b.

We have also attempted to create quasi-independent hindcasts of the rainfall, shown by the dotted line. This involves calculating SST EOFs over a period independent of the rainfall and forming multiple regression equations for these independent periods. A problem is that some of the lower LF SST EOFs of interest become confounded in some of these periods. This applies mainly to EOF4 which can be confounded with EOF5. So we have allowed up to 5 EOFs in the multiple regression formulae but have only retained those that are statistically significant. We have, experimentally, hindcast for 15 year periods at a time in this way. These were chosen to be 1901-1915, 1916-1930, 1931-1945, 1946-1960, 1961-1975, 1976-1990. In choosing these periods we are constrained by the need to keep as many years as possible for calculating LF SST EOFs The hindcasts are little different from the simulations (better before 1930), except that for 1946-60 which completely fails to pick up the increase in rainfall to the 1950 peak.

6. Discussion and conclusions.

There are divergent opinions regarding the importance of tropical and midlatitude processes in the interdecadal variations of oceanic and atmospheric climate in the Pacific sector. On the one hand, Graham (1994), suggests that changes in tropical Pacific SST and convection are important in forcing the observed decadal-scale variations in atmospheric circulation at midlatitudes, even though the midlatitude SST anomalies induced by the anomalous atmospheric circulation may provide further positive feedback (Lau, 1997). Knutson and Manabe (1997) find that low-latitude oceanic mechanisms drive both the conventional El Niño and bidecadal variations of tropical and subtropical Pacific SST in atmosphere-ocean model simulations. On the other hand, Latif and Barnett (1996) find strong evidence that the interdecadal variations of SST in midlatitudes are a result of ocean-atmosphere interactions involving the subtropical ocean gyre and the Aleutian low, without an important contribution from tropical SST anomalies. Our results lend support to the latter view to the extent that our first two LF SST EOFS do not include important variations in

equatorial SST. However tropical SST anomalies on interannual time scales may provide a key triggering role through their influence on the extratropical atmospheric circulation (Trenberth and Hurrell, 1994). In addition, Gu and Philander (1997) have proposed that subduction and equatorward transport of subtropical Pacific surface waters may provide a mechanism for oceanic fluctuations on interdecadal time scales, along with interactions between the tropical Pacific Ocean and the tropical and extratropical atmosphere. Our LF EOF3 certainly indicates the possibility of a more active interaction between the extratropical and tropical ocean in the Pacific. On the interannual ENSO time scales, the extratropical parts of the SST patterns like Fig. 6a (HF EOF1) are often regarded as largely a response to tropical forcing. Relative to its equatorial weights, the extratropical weights of LF EOF3 are more than three times stronger than for HF EOF1. It is not completely clear whether this represents a more active tropical-extratropical Pacific Ocean interaction on bidecadal and longer time scales, or merely a coincidence of time scales of SST variation of reverse phase.

Another approach (Currie, 1996; White et al., 1997) has been to ascribe bidecadal climate variability to lunar tidal or "Hale Cycle" solar influences. A hypothesis involving the lunar 18-year tidal time scale or the 22-year Hale Cycle, however, does not explain the greater importance of bidecadal variability in the Pacific than in the Atlantic. Furthermore, if the dominant frequency bands of ocean-atmosphere interactions overlap with the frequencies of external (lunar or solar) forcings, the origins of bidecadal climate variations are likely to be misinterpreted in the absence of thorough, physically-based, sensitivity studies. However solar influences may be enhanced through forced stratospheric ozone fluctuations (Haigh, 1996). So the energetics of hypothesized triggering by lunar tidal and solar influences still need to be assessed. White et al. (1997) claim that the magnitudes and phases of worldwide decadal and bidecadal variations in SST are consistent with those of 11-year cycle and Hale-Cycle solar forcing respectively, but they do not explain the greater bidecadal variability in the Pacific and greater decadal variability in the Atlantic, even though this is evident in their Fig. 6.

It is likely that there are several "quasi bidecadal" phenomena. Identifying the several physical processes likely to exist on these time scales requires the use of coupled models, atmospheric models and observations. Our results indicate that more than one near bidecadal to multi decadal pattern of SST is likely to have a strong influence on the best known near bidecadal variations of climate, those of Southern African rainfall. Considering that rainfall tends to be strongly affected by chaotic internal atmospheric processes, we believe our results are noteworthy. Thus much more analysis of LF rainfall (e.g. Eastern Australia, Fig. 8; western USA, not shown) and temperature (e.g. New Zealand) in key regions influenced on decadal to multidecadal time scales is needed. We plan this in tandem with model simulations for the last century using the more realistic pre-1950 GISST data sets now available (e.g. Rayner et al, 1997 and personal communication) and new analyses of worldwide surface pressure since the 1870s (Basnett and Parker, 1997).

Acknowledgements.

The rainfall data set provided by M. Hulme (Climatic Research Unit, University of East Anglia), was developed with the support of the U.K. Department of the Environment under Contract No. PECD/7/10/198.

APPENDIX 1

ENHANCEMENT OF EOF TIME SERIES FOR MISSING DATA.

Consider a fixed spatial pattern of eigenvector weights $\underline{A}_k$. Let there be m weights with the weight at a point I being A_{ki}. If the field of data X_{it} is complete, the true time coefficient is Z_{kt} such that

$$Z_{kt} = \sum_{i=1}^{m} A_{ki} X_{it} \qquad (1a)$$

But if some data are missing, we cannot calculate Z_{kt} as in equation 1 because we do not know all the X_{it}. The usual method is to ignore this problem and calculate $Z^{\cdot}_{kt}$ from the available data $i^{\cdot}$. Writing Z'_{kt} as the contribution from the missing data that we wish to estimate then

$$Z_{kt} = Z'_{kt} + Z^{\cdot}_{kt} \qquad (1b)$$

where

$$Z^{\cdot}_{kt} = \sum_{i^{\cdot}} A_{ki^{\cdot}} X_{i^{\cdot}t}$$

and

$$Z'_{kt} = \sum_{i'} A_{ki'} X_{i't} \qquad (1c)$$

Because missing data points progressively increase in amount in earlier times, it would be expected from Equation 1a that the variance of an EOF time series $Z^{\cdot}_{kt}$ would tend to reduce systematically, though details would depend on the distribution of missing data. We now make nearly unbiased estimates of the influence of missing data from the time series of the leading eigenvectors. We make these estimates from a function of the spatial weights at missing data points as follows. The actual but unknown value of a missing observation at time t is

$$X_{i't} = \sum_{K=1}^{m} A_{i'k} Z_{kt} \qquad (2)$$

Substitute (2) into (1c)

$$Z'_{kt} = \sum_{i'} A_{ki'} X_{i't} = \sum_{i'} A_{ki'} \sum_{j=1}^{m} A_{i'j} Z_{jt}$$

Substituting for Z_{jt} from (1b) with a small amount of manipulation gives

$$Z'_{kt} = \sum_{j=1}^{m} \left(\sum_{i'} A_{ki'} A_{i'j} \right) (Z'_{jt} + Z^{*}_{jt})$$

Now $\sum_{i'} A_{ki'} A_{i'j}$ is a constant at a given time that depends on the sum of the product of the weights of EOF k, and the weights of the m EOFs including EOF k, for each missing data point. This constant, C'_{kjt} varies through time as the distribution of missing data varies. Thus

$$Z'_{kt} = \sum_{j=1}^{m} C'_{kjt} \; (Z'_{jt} + Z^{*}_{jt}) \qquad (3a)$$

This is true for all m EOFs. The higher order EOFs are likely to be noise. So although the above model does not have an explicit noise term we filter noise by including only the first m <M EOFs where M is total number of EOFs. We can rewrite (3a) for all m EOFs using the one dimensional matrices $\underline{Z}'_t$ and $\underline{Z}^{*}_t$ as:

$$\underline{Z}'_t = \underline{C}'_t \; (\underline{Z}'_t + \underline{Z}^{*}_t) \qquad (3b)$$

This is easily shown to give:

$$\underline{Z}_t = (\underline{I}_t - \underline{C}'_t)^{-1} \; \underline{Z}^{*}_t \qquad (4)$$

Here we use m=10. Thus for LF EOFs we use the first 10 LF EOFs to do the enhancement and for HF EOFs we use the first 10 HF EOFS. Fig A1 shows time series of LF SST EOF4 before and after enhancement (m=10) and for m=4 and 8. The increase in signal magnitude before 1900, and a change in the First World War, is clear. An additional problem with LF EOFs is that the enhanced EOF time series is affected by the timing of data gaps. This creates a small but discernible amount of HF noise in the reconstructions. This is smoothed by reapplying the 13 year low pass filter to the initial version of the reconstructed time series.

References

Allan, R, Lindesay, J. and Parker, D.E., 1996: *El Niño Southern Oscillation and Climatic Variability*. CSIRO Publishing, 416pp.

Allen, M.R. and L.A. Smith, 1996, Monte Carlo SSA: Detecting irregular oscillations in the presence of coloured noise. *J. Climate*, 3373-3404.

Basnett, T.A. and Parker, D.E., 1997: Development of the Global Mean Sea Level Pressure Data Set GMSLP2. *Climate Research Technical Note 79*, Hadley Centre, Meteorological Office, Bracknell, U.K.

Bottomley, M., Folland, C.K., Hsiung, J., Newell, R.E. and Parker, D.E., 1990: *Global Ocean Surface Temperature Atlas (GOSTA)*. Joint Meteorological Office and Massachusetts Institute of Technology Project, supported by US Dept. of Energy, US National Science Foundation and US Office of Naval Research and funded by UK Depts of the Environment and Energy. HMSO, London. 20 + iv pp and 313 Plates.

Chang, P., Ji, L. and Li, H., 1997: A decadal climate variation in the tropical Atlantic Ocean from thermodynamic air-sea interactions. *Nature*, **385**, 516-518.

Cockcroft, M.J., Wilkinson, M.J. and Tyson, P.D., 1987: The application of a present-day climatic model to the late Quaternary in southern Africa, *Climatic Change*, **10**, 161-181.

Cohen, A.L. and Tyson, P.D., 1995: Sea-surface temperature fluctuations during the Holocene off the south coast of Africa: implications for terrestrial climate and rainfall. *The Holocene*, **5**, 304-312.

Currie, R.G., 1996: Variance contribution of luni-solar (M_n) and solar cycle (S_c) signals to climate data. *Int. J. Climatol.*, **16**, 1343-1364.

Deser, C. and Blackmon, M.L., 1993: Surface climate variations over the North Atlantic Ocean during winter: 1900-1989. *J. Climate*, **6**, 1743-1753.

Folland, C.K., Parker, D.E. and Palmer. T.N. 1986: Sahel rainfall and worldwide sea temperatures 1901-85. *Nature*, **320**, pp602-607.

Folland, C.K., Owen, J., Ward, M.N. and Colman, A., 1991: Prediction of seasonal rainfall in the Sahel region using empirical and dynamical methods. *J. Forecasting*, **10**, 21-56.

Folland, C.K., Colman, A., Salinger, M.J. and Parker, D.E., 1993: Eigenvectors of Global Sea Surface Temperature and night marine air temperature, 1901-90, and relationships with New Zealand Air temperature, 1871-1992. *Proc. Fourth Int. Conf. on Southern Hem. Meteorology and Oceanography, Hobart, Tasmania, 29 Mar- 2 Apr 1993*, 322-323.

Folland, C.K. and Parker, D.E., 1995: Correction of instrumental biases in historical sea surface temperature data. *Quart. J. Roy. Meteorol. Soc.*, **121**, 319-367.

Folland, C.K., Parker, D.E. and Kates, F.E., 1984: Worldwide marine temperature fluctuations 1856-1981. *Nature*, **310**, 670-673.

Folland, C.K. and Salinger, M.J., 1995: Surface temperature trends and variations in New Zealand and the surrounding ocean, 1871-1993. *Int. J. Climatol.*, **15**, 1195-1218.

Folland C.K., Salinger, M.J. and Rayner, N., 1997: Annual South Pacific island air temperatures and ocean surface temperatures. *N.Z. J. Weather and Climate*, **17(1)**, *23-42.*

Ghil, M. and Vautard, R., 1991: Interdecadal oscillations and the warming trend in global temperature time series. *Nature*, **350**, 324-327.

Graham, N.E., 1994: Decadal-scale variability in the tropical and North Pacific during the 1970s and 1980s: observations and model results. *Clim. Dyn.*, **10**, 135-162.

Gu, D. and Philander, S.G.H., 1997: Interdecadal climate fluctuations that depend on exchanges between the tropics and extratropics. *Science*, **275**, 805-807.

Haigh, J.D., 1996: The impact of solar variability on climate. *Science,* **272**, 981-984.

Hulme, M., 1994: Validation of large-scale precipitation fields in General Circulation Models. In *Global precipitations and climate change*, M. Desbois and F. Désalmand (eds), Springer-Verlag, pp387-405.

Kachi, M. and Nitta, T., 1997: Decadal variations of the global atmosphere-ocean system. *J. Met. Soc. Japan*, **75**, 657-675.

Kawamura, R., 1994: A rotated EOF analysis of global sea surface temperature variability with interannual and interdecadal time scales. J. *Phys. Oceanog.*, **24**, 707-715.

Kim, K-Y., 1996: Temporal and spatial subsampling errors for global empirical orthogonal functions: Applications to surface temperature field. *J. Geophys. Res.*, **101,** 23433-23446.

Kleeman, R., Colman, R.A., Smith, N.R. and Power, S.B., 1996: A recent change in the mean state of the Pacific basin climate: observational evidence and atmospheric and oceanic responses. *J. Geophys. Res.*, **101**, 20483-20499.

Knutson, T.R. and Manabe, S., 1997: Model assessment of decadal variability and trends in the tropical Pacific Ocean. Submitted to *J. Climate.*

Kushnir, Y., 1994: Interdecadal variations in North Atlantic sea surface temperature and associated atmospheric conditions. *J. Climate*, **7**, 141-157

Latif, M. and Barnett, T.P., 1996: Decadal climate variability over the North Pacific and North America: dynamics and predictability. *J. Climate*, **9**, 2407-2423.

Latif, M., Kleeman, R. and Eckert, T.P., 1997: Greenhouse warming, decadal variability or El Nino? An attempt to understand the anomalous 1990s. *J. Climate*, **10**, 2221-2357.

Lau, N-C., 1997: Interactions between global SST anomalies and the midlatitude atmospheric circulation. *Bull. Amer. Meteorol. Soc.*, **78**, 21-33.

Mann, M.E. and Park, J., 1994: Global-scale modes of surface temperature variability on interannual to century timescales. *J. Geophys. Res.*, **99**, 25819-25833.

Mann, M.E. and Park, J., 1996: Joint spatio-temporal modes of surface temperature and sea level pressure variability in the Northern Hemisphere during the last century. *J. Climate*, **9**, 2137-2162.

Mantua, N.J., Hare, S.R., Zhang, Y., Wallace, J.M. and Francis, R.C., 1997: A Pacific Interdecadal climate oscillation with impacts on salmon production. *Bull. Amer. Met. Soc.*, 78, 1069-1079.

Newell, N.E., Newell, R.E., Hsiung, J. and Wu, Z-X., 1989: Global marine temperature variation and the solar magnetic cycle. *Geophys. Res. Lett.*, **16**, 311-314.

Nitta, T., and Kachi, M., 1994: Interdecadal variations of precipitation over the tropical Pacific and Indian Oceans. *J. Met. Soc. Japan*, **72**, 823-831.

Parker, D.E. and Folland, C.K., 1991: Worldwide surface temperature trends since the mid-19th century. In *Greenhouse-Gas-Induced Climatic Change: A Critical Appraisal of Simulations and Observation*, M.E.Schlesinger (ed.), Elsevier, pp 173-193.

Parker, D.E., Jones, P.D., Folland, C.K. and Bevan, A., 1994: Interdecadal changes of surface temperature since the late nineteenth century, *J. Geophys. Res.* **99**, 14373-14399.

Parker, D.E., Folland, C.K. and Jackson, M., 1995a: Marine surface temperature: observed variations and data requirements. *Climatic Change*, **31**, 559-600.

Parker, D.E., Jackson, M. and Horton, E.B., 1995b: The GISST2.2 sea surface temperature and sea-ice climatology. *Climate Research Technical Note 63*, Hadley Centre, Meteorological Office, Bracknell, U.K., 35pp.

Parker, D.E., Folland, C.K., Bevan, A., Ward, M.N., Jackson, M. and Maskell, K. 1995c: Marine surface data for analysis of climatic fluctuations on interannual to century time scales. In: *"Natural Climate Variability on Decade-to-Century Time Scales"* Eds: D.G. Martinson, K. Bryan, M.Ghil, M.M. Hall, T.R. Karl, E.S. Sarachik, S.Sorooshian and L.D.Talley. National Acad. Press, Washington, DC. pp241-250. Colour figs pp222-228.

Rasmusson, E.M. and Carpenter, T.H., 1982: Variations in tropical sea surface temperature and surface wind fields associated with the Southern Oscillation/El Nino. *Mon. Weath. Rev.*, 110, 354-384.

Rayner, N.A., Horton, E.B., Parker, D.E., Folland, C.K. and Hackett, R.B., 1996:

Version 2.2 of the Global sea-Ice and Sea Surface Temperature data set, 1903-1994. *Climate Research Technical Note CRTN74*, Hadley Centre, Meteorological Office, Bracknell, U.K., 35pp.

Ropelewski, C.F. and Jones, P.D., 1987: An extension of the Tahiti-Darwin Southern Oscillation Index. *Mon. Weath. Rev.*, **115**, 2161-2165.

Schlesinger M.E. and Ramankutty,N., 1994: A oscillation in the global climate system of period 65-70 years. *Nature*, 367, 723-726.

Trenberth, K.E. and Hurrell, J.W., 1994: Decadal atmosphere-ocean variations in the Pacific. *Clim. Dyn.*, **9**, 303-319.

Tyson, P.D., 1991: Climatic change in southern Africa: past and present conditions and possible future scenarios. *Climatic Change*, **18**, 241-258.

Tyson, P.D. and Dyer, T.G.J.,1980: The likelihood of droughts in the eighties in South Africa, *S. African J. of Science*, **76**, 340-341.

Tyson, P.D., Dyer, T.G.J. and Mametse, M.N., 1975: Secular changes in South African rainfall: 1880 to 1972, *Quart. J. Roy. Meteorol. Soc.*, **101**, 817-833.

Tyson, P.D. and Lindesay, J.A., 1992: The climate of the last 2000 years in southern Africa. *The Holocene*, **2**, 271-278.

Venegas, S.A., Mysak, L.A. and Straub, D.N., 1996: Evidence for interannual and interdecadal climate variability in the South Atlantic. *Geophys. Res. Lett.*, **23**, 2673-2676.

Ward, M.N., Maskell, K., Folland, C.K., Rowell, D.P. and Washington, R., 1994: A tropic-wide oscillation of boreal summer rainfall and patterns of sea-surface temperature. *Climate Research Technical Note CRTN48*. Hadley Centre, Meteorological Office, Bracknell, U.K., 29pp.

White, W.B., Lean,J., Cayan, D.R. and Dettinger, M.D., 1997: Response of global upper ocean temperature to changing solar irradiance. *J. Geoph. Res.*, **102**, 3255-3266.

Young, P.C., Ng, C.N., Lane, K. and Parker, D.E., 1991: Recursive forecasting, smoothing and seasonal adjustment of non-stationary environmental data. *J. Forecasting*, **10**, 57-89.

Zhang, Y., Wallace, J.M. and Battisti, D.S., 1997: ENSO-like interdeacadal variability: 1900-1993. *J. Climate*, 1004-1020.

Figure Captions

Figure 1 Seasonal (January to March, etc.) anomalies of SST (solid line) and NMAT (dashed line) relative to 1961-1990 climatology, 1861-1996. The smooth curves are filtered to pass >50% of the variance at periods >13.3 years. **a)** Globe: **b)** Northern Hemisphere; **c)** Southern Hemisphere; **d)** Tropics (20°N -20°S); **e)** Atlantic 0°-20°S; **f)** North Pacific (0°-65°N, 120°E to American coast); **g)** South Pacific (0°-50°S, 120°E to American coast); **h)** Indian Ocean north of 50°S.

Figure 2 Power spectra of detrended annual anomalies of SST (heavy solid) and NMAT (light solid), relative to 1961-1990 climatology. The analysis period is 1876-1996 unless otherwise specified. The dashed lines (thick, SST; thin, NMAT) are upper 95% confidence limits for Markov red noise. **a)** Globe: **b)** Northern Hemisphere; **c)** North Atlantic(0°-80°N, excluding Mediterranean but including Arctic to 70°E); **d)** North Pacific (0°-65°N, 120°E to American coast); **e)** Southern Hemisphere; **f)** Southern Hemisphere 0°-40°S; **g)** Atlantic 0°-20°S; **h)** South Pacific (0°-50°S, 120°E to American coast); **I)** North Indian Ocean; **j)** Warm pool 15°N -10°S, 65°-180° E; **k)** Western tropical Pacific 20°N -20°S, 120° E-170° W, 1898-1996; **l)** Northern tropics (0°-20°N); **m)** Indian Ocean 0°-50°S; **n)** Nino 3.4 area (5°N -5°S, 120°-170° W); **o)** Nino 1 + 2 area (0°-10°S, 80°-90°W, 1906-1996) **p)** Southern tropics (0°-20°S). Vertical dashed lines show periods of 15 and 24 years.

Figure 3 a) Standard deviation of low-pass filtered SST anomalies for the period 1911-1995 falling in the bidecadal range (approximately 18-30 years). **b)** as a) but expressed as a percentage of the total low-pass (>13 years) variance. **c), d)** as a), b) but for range of periods prominent in New Zealand temperature (approximately 13-18 years).

Figure 4 a) Pattern of weights of LF SST EOF1, 1911-1995. **b)** Linear trends of SST, 1911-1995 **c)** Time-series of LF SST EOF1, 1861-1996. Global mean SST anomalies are shown as a dashed line. **d), e)** as a), c) but for LF SST EOF2. **f), g)** as a), c) but for LF SST EOF3 **h)** FFT power spectrum of LF EOF3. **I),j),k)** as **f),g),h)** but LF SST EOF4.

Figure 5 a) Pattern of weights of LF EOF3 MOHMAT4N2 NMAT for 1911-1995. **b)** Time-series corresponding to a), 1861-1996.

Figure 6 a). Pattern of weights of HF SST EOF1 for 1911-1995 (see text). **b)** As a) but for HF SST. **c)** Time-series of HF EOF1 (heavy line) and HF EOF2 (light line) plotted seasonally. **d)** Lag correlations between HF EOF1 and HF EOF2. Positive lag implies EOF1 leads EOF2.

Figure 7 Pattern of weights of extended LF EEOF3 for 1911-1995 for **a)** April-June **b)** July-September **c)** October-December **d)** for 1912-1996 for January-March.

Figure 8 Correlations between LF SST EOF3 time series in Fig. 4g and correspondingly LF gridded rainfall in **a)** January to March and **b)** July to September, 1901-1995. Bold values are significantly different from zero at the 95% level of confidence.

Figure 9 a) Pattern of unfiltered EOF1 of rainfall for 20^0N to 40^0S, January-March 1901-1995. **b)** time series of January-March unfiltered rainfall EOF1 (solid line) and HF SST EOF1 (dashed line), 1900-1995 **c)** FFT spectrum of January-March unfiltered rainfall EOF1 **d)** pattern of unfiltered rainfall EOF1 for 40^0N to 20^0S, July-September 1901-1995. **e)** as b, but July-September. **f)** As c. but July-September. In the spectra, dashed lines are the upper 95% confidence limits. Rainfall EOFs were calculated using the same equal-area box scheme as for SST and NMAT, but, to qualify for analysis, an equal-area box required at least one constituent 5^0x5^0 box to have at least 50% of seasons with data in all 3 months. Vertical dashed lines show periods of 15 and 24 years.

Figure 10 a). (Solid line) Time series of LF rainfall for southern Africa, January-March, 1900-1991. (Dashed line) Simulated rainfall using a stepwise multiple regression of LF SST EOFs 2, 3 and 4. (Dotted line) Hindcast rainfall using a jackknife method in 15 year blocks (see text). **b)** Difference in detrended LF sea surface temperature between the wettest 25% and driest 25% of values of LF southern African rainfall, 1900-1991.

Figure A1 Time series of LF EOF4 before and after enhancement, 1861-1995.

Figure 1

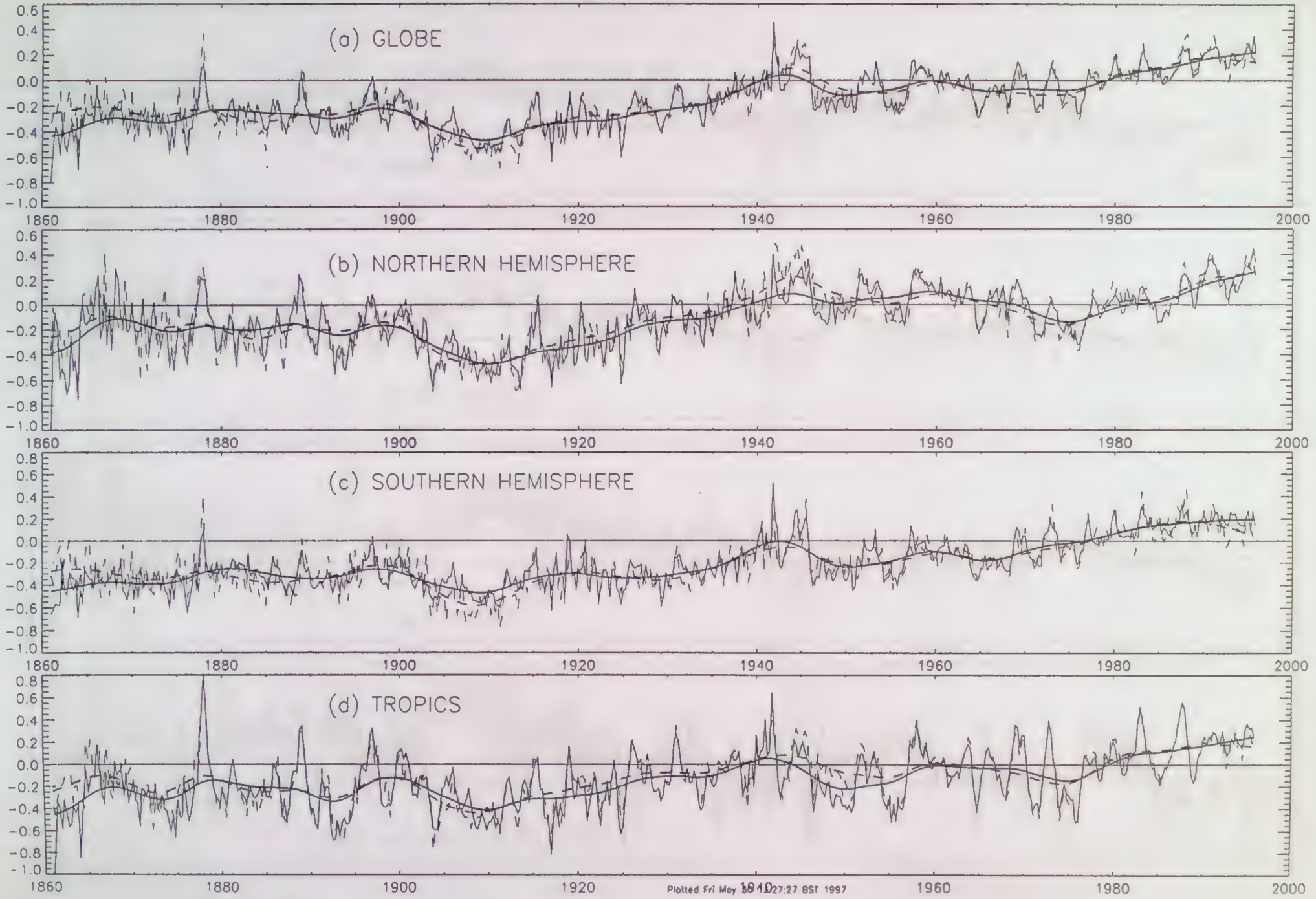
(a) GLOBE
(b) NORTHERN HEMISPHERE
(c) SOUTHERN HEMISPHERE
(d) TROPICS
1860
1880
1900
1920
1940
1960
1980
2000
Plotted Fri May 30 10:27:27 BST 1997

Figure 1 cont

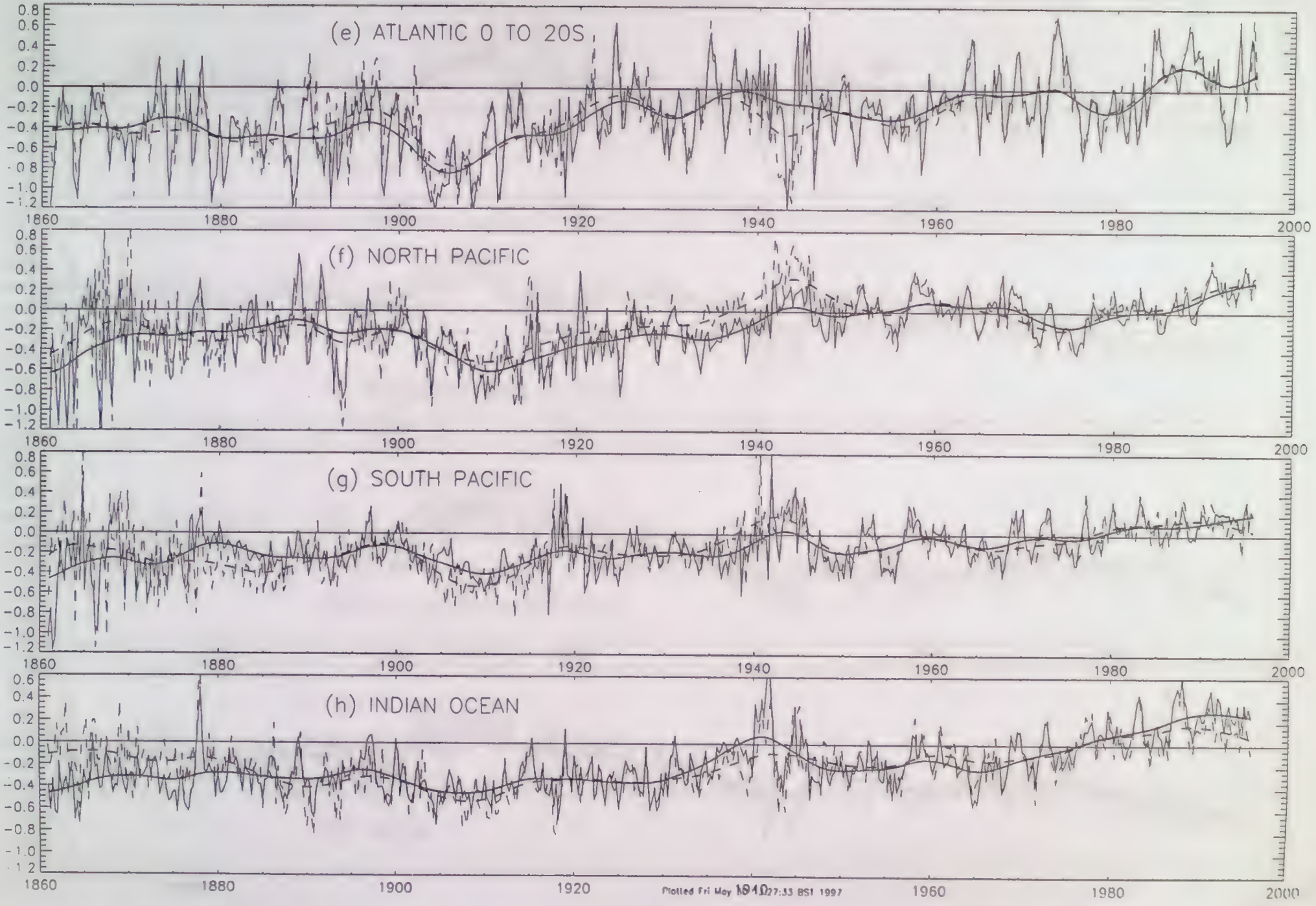

Figure 2

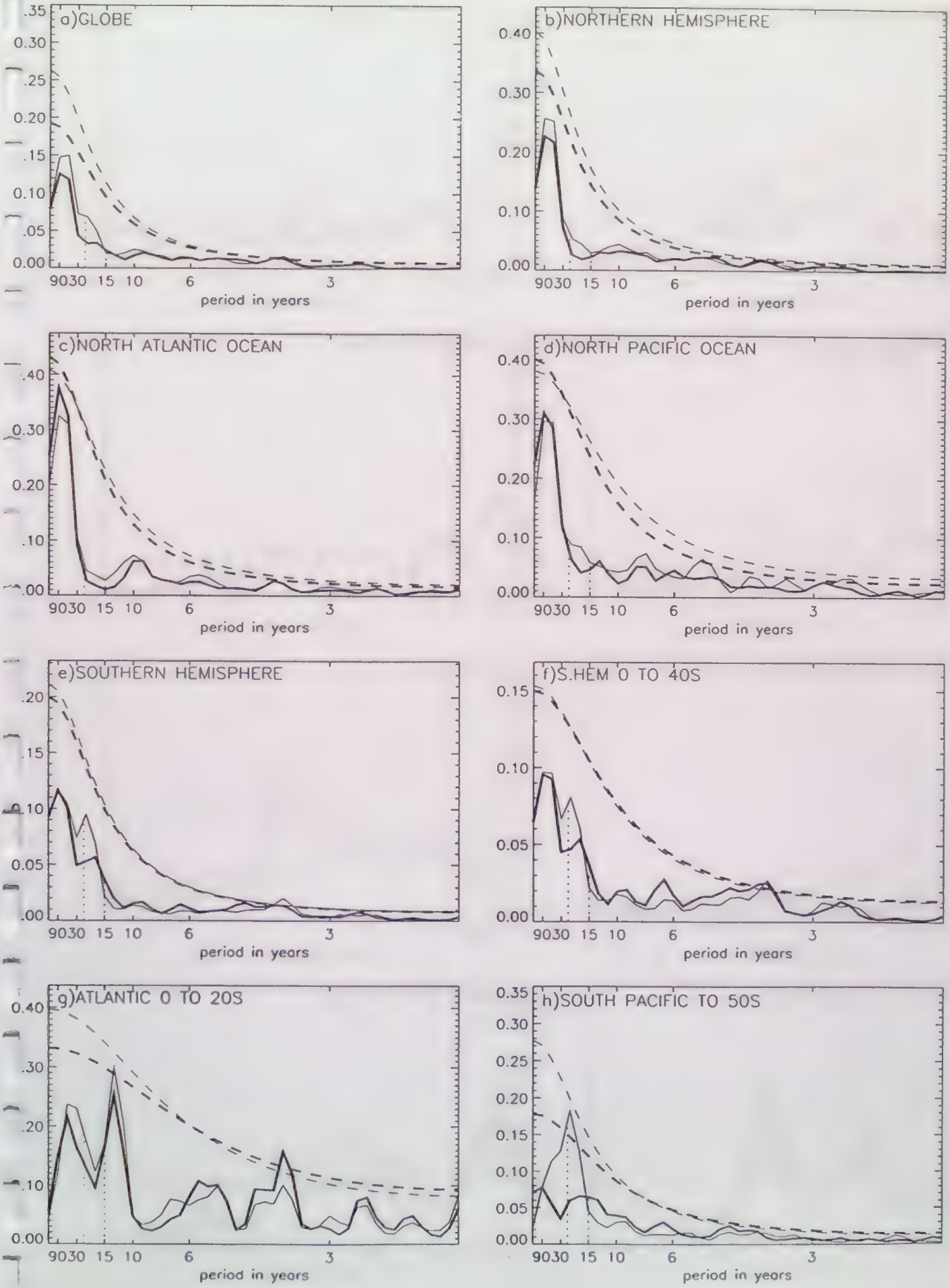
a)GLOBE
b)NORTHERN HEMISPHERE
c)NORTH ATLANTIC OCEAN
d)NORTH PACIFIC OCEAN
e)SOUTHERN HEMISPHERE
f)S.HEM 0 TO 40S
g)ATLANTIC 0 TO 20S
h)SOUTH PACIFIC TO 50S
9030 15 10 6 3
period in years

Figure 2 cont

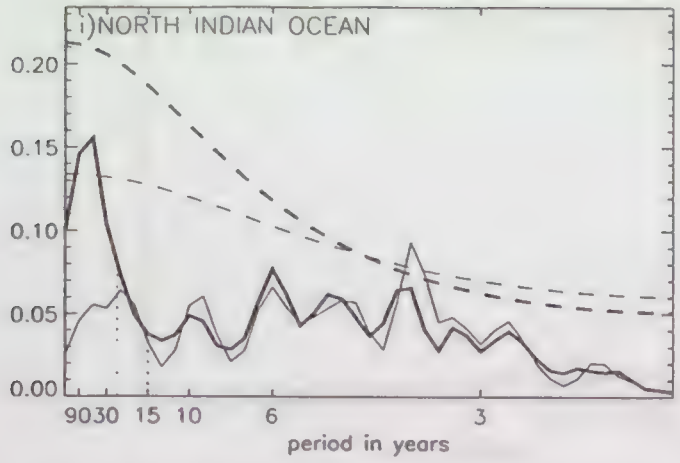

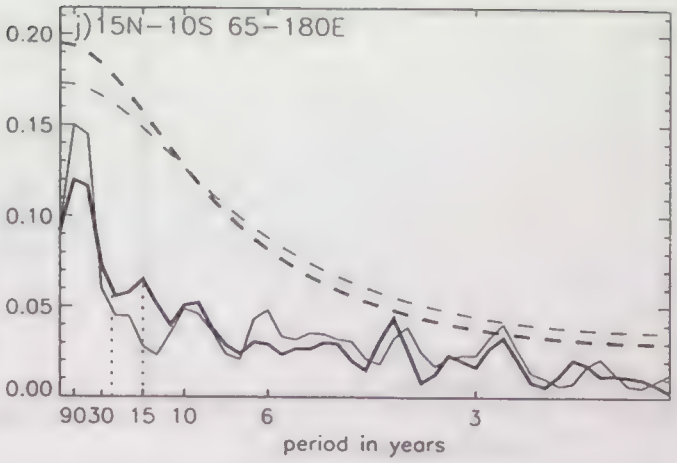

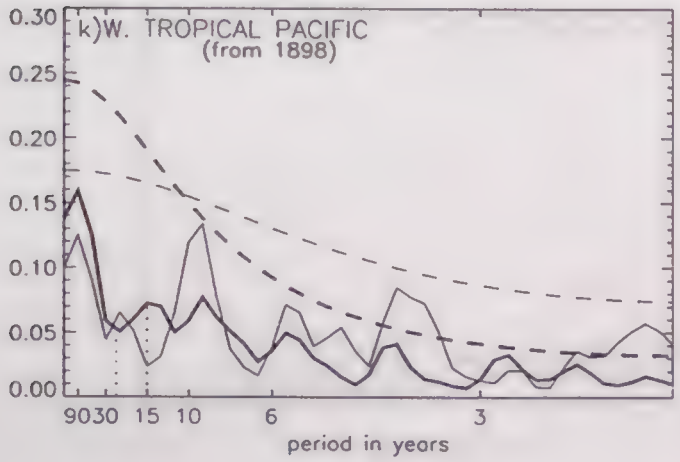

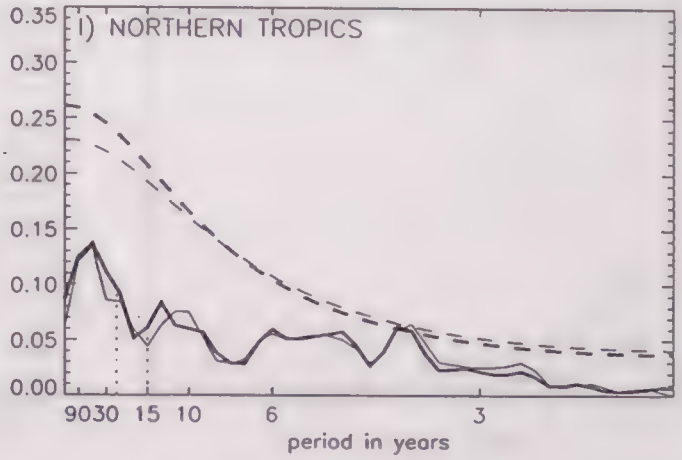

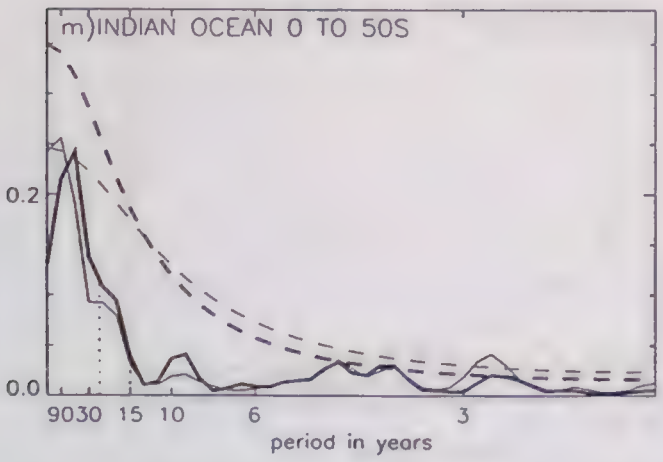

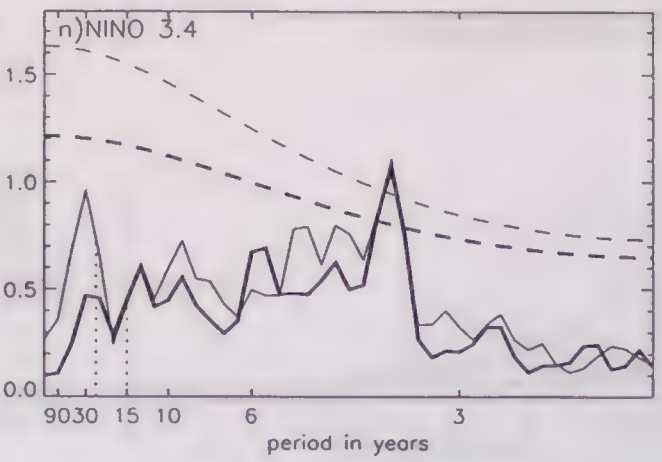

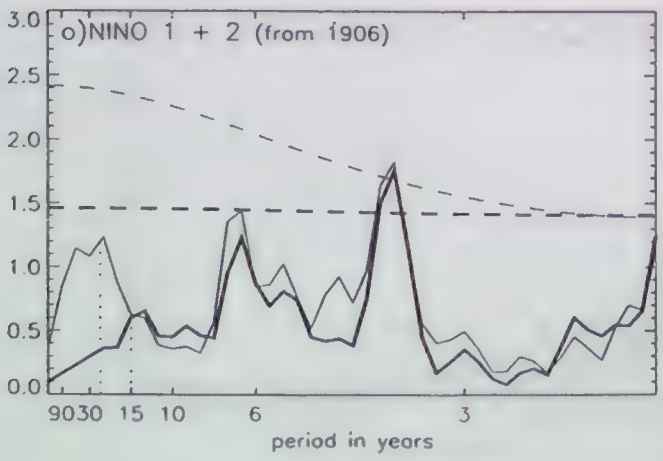

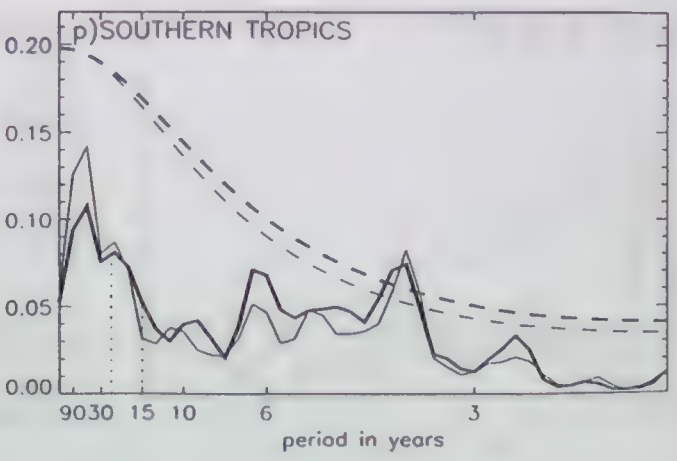

Figure 3

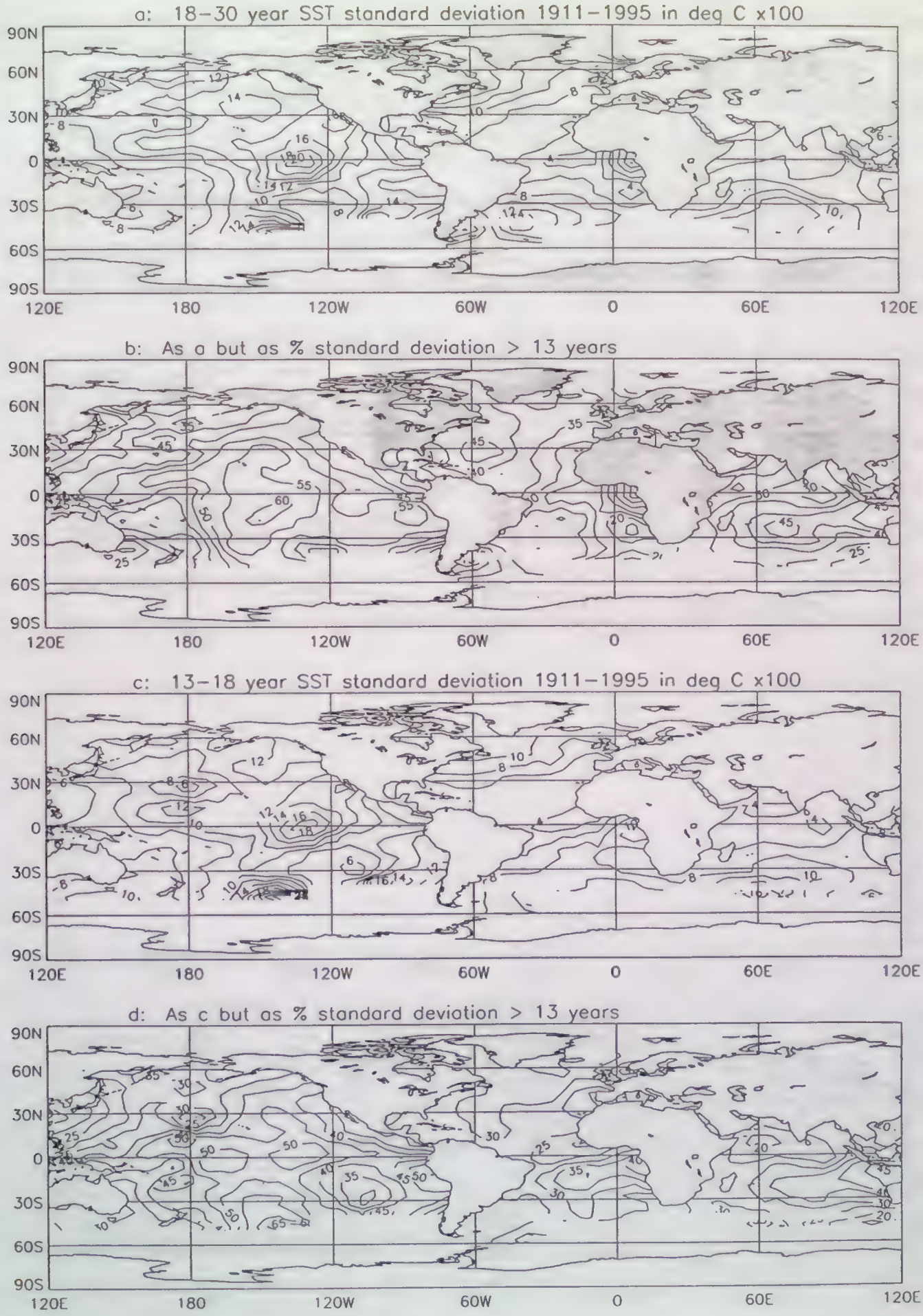
a: 18–30 year SST standard deviation 1911–1995 in deg C x100
b: As a but as % standard deviation > 13 years
c: 13–18 year SST standard deviation 1911–1995 in deg C x100
d: As c but as % standard deviation > 13 years
90N
60N
30N
0
30S
60S
90S
120E
180
120W
60W
0
60E
120E

Figure 4

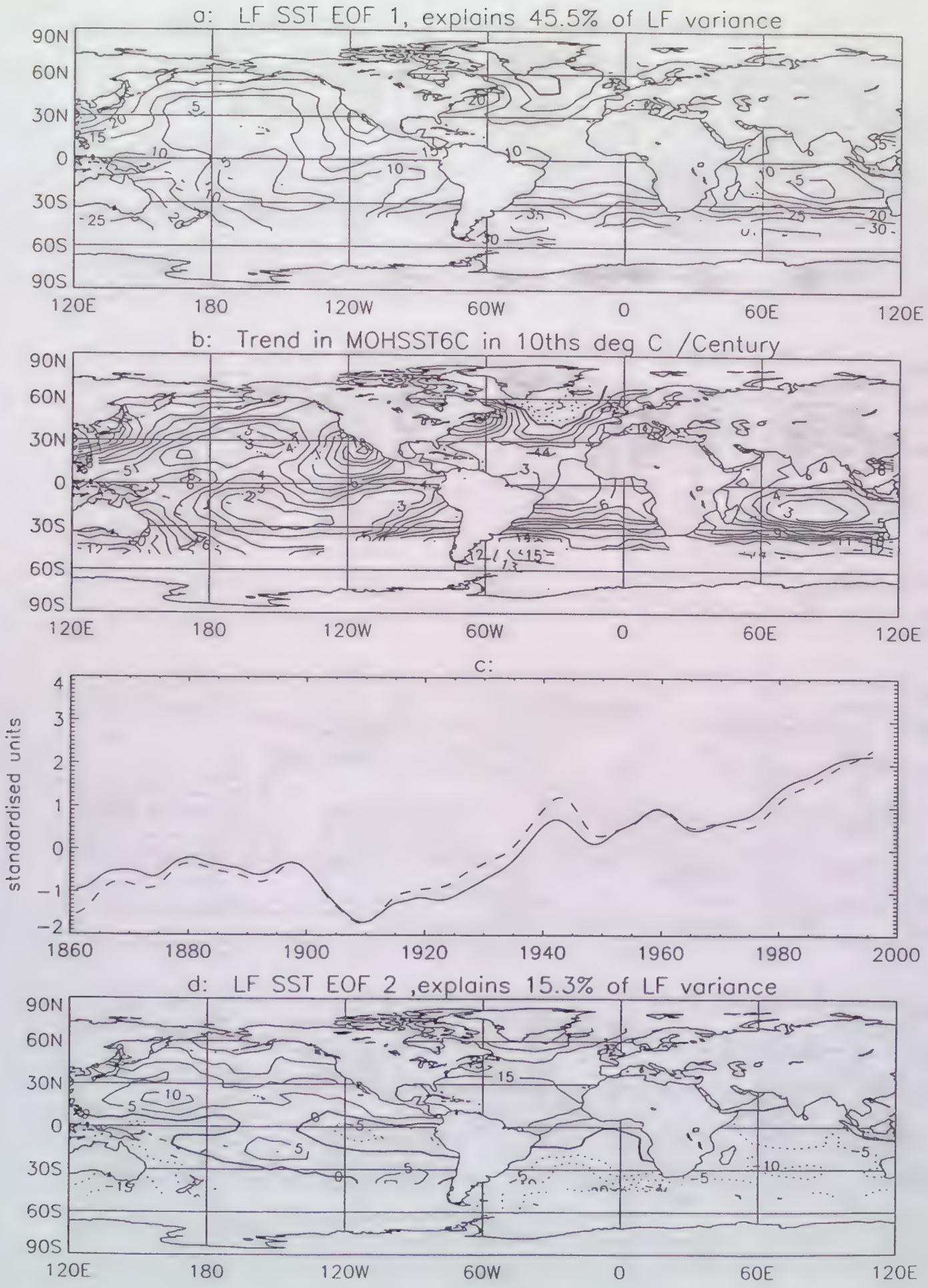
a: LF SST EOF 1, explains 45.5% of LF variance
90N
60N
30N
0
30S
60S
90S
120E
180
120W
60W
0
60E
120E
b: Trend in MOHSST6C in 10ths deg C /Century
c:
standardised units
4
3
2
1
0
−1
−2
1860
1880
1900
1920
1940
1960
1980
2000
d: LF SST EOF 2 ,explains 15.3% of LF variance

Figure 4 cont

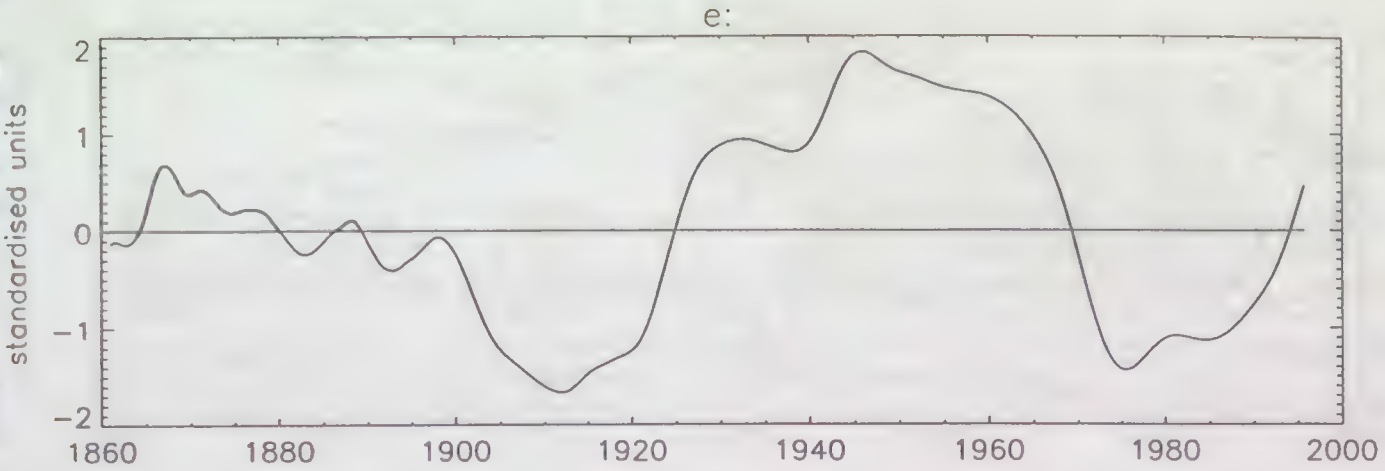

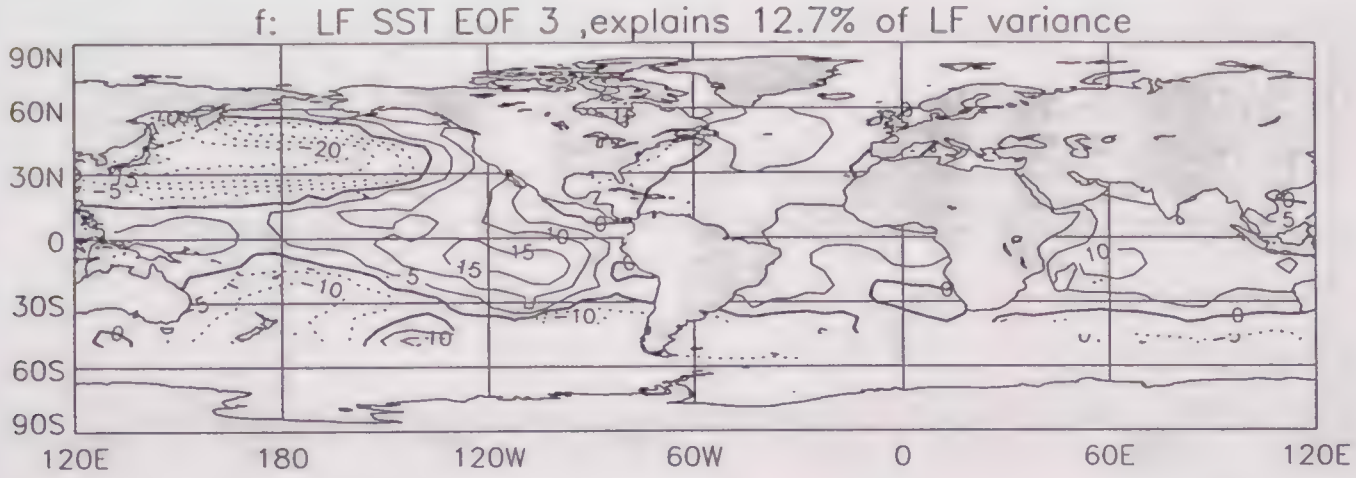

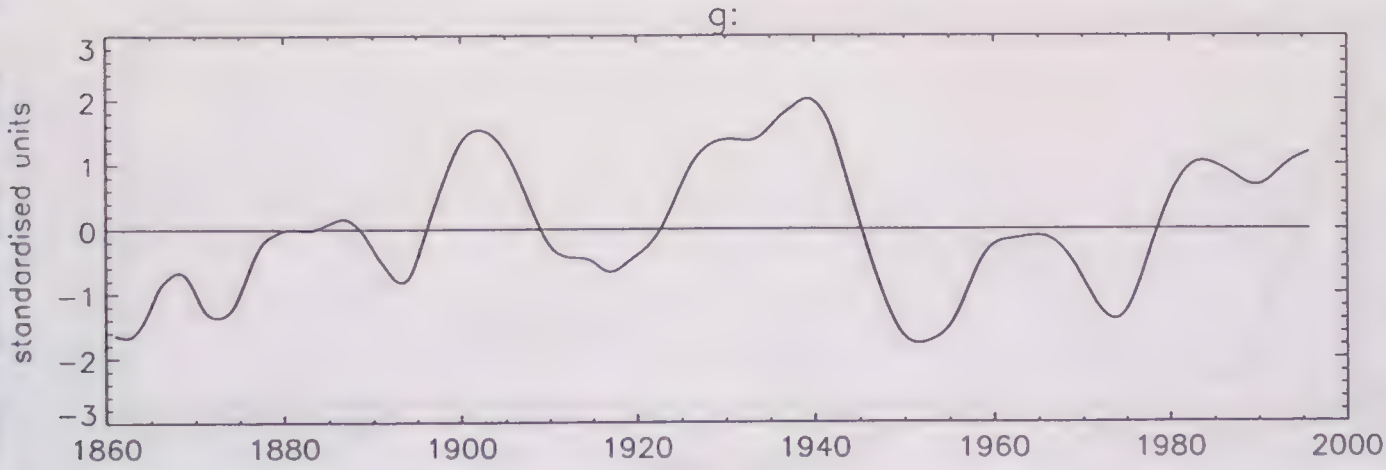

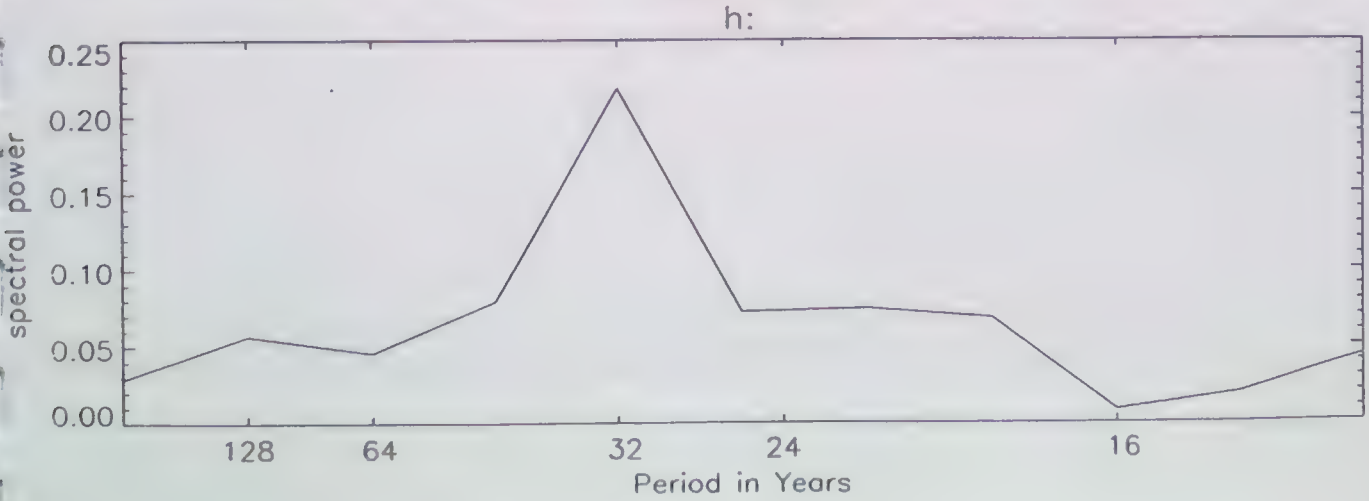

Figure 4 cont

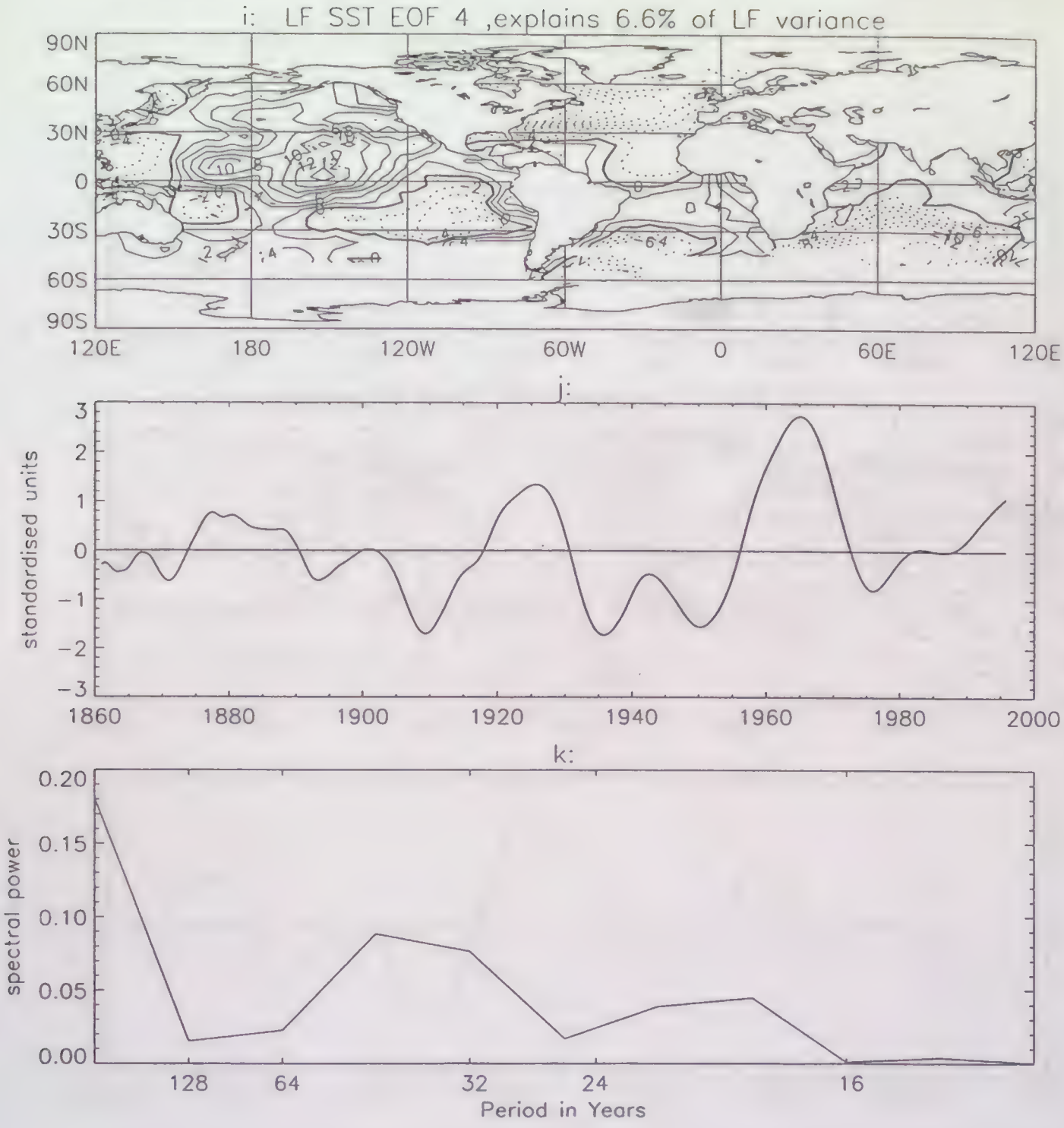

Figure 5

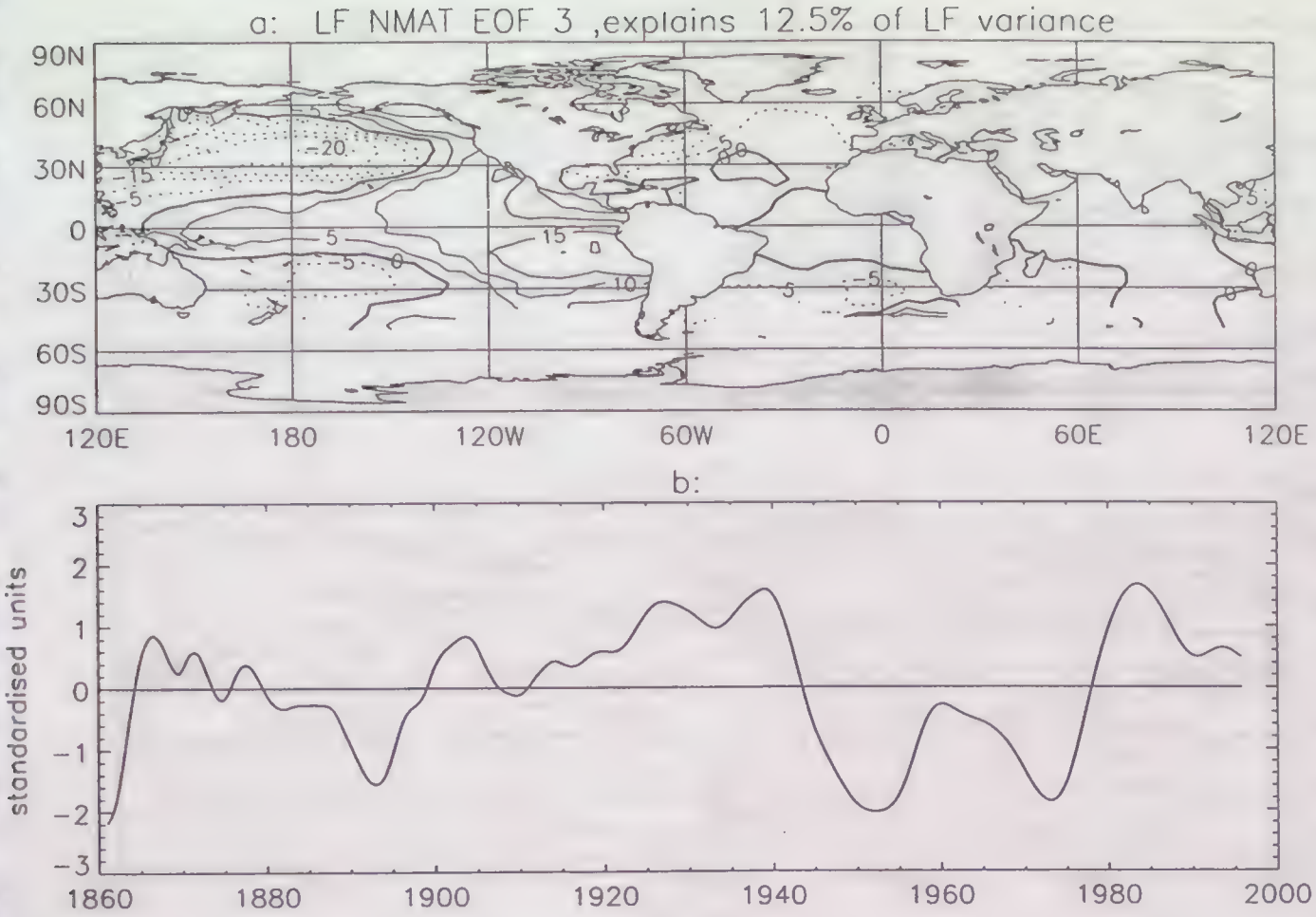
a: LF NMAT EOF 3 ,explains 12.5% of LF variance
90N
60N
30N
0
30S
60S
90S
120E
180
120W
60W
0
60E
120E
b:
standardised units
3
2
1
0
−1
−2
−3
1860
1880
1900
1920
1940
1960
1980
2000

Figure 6

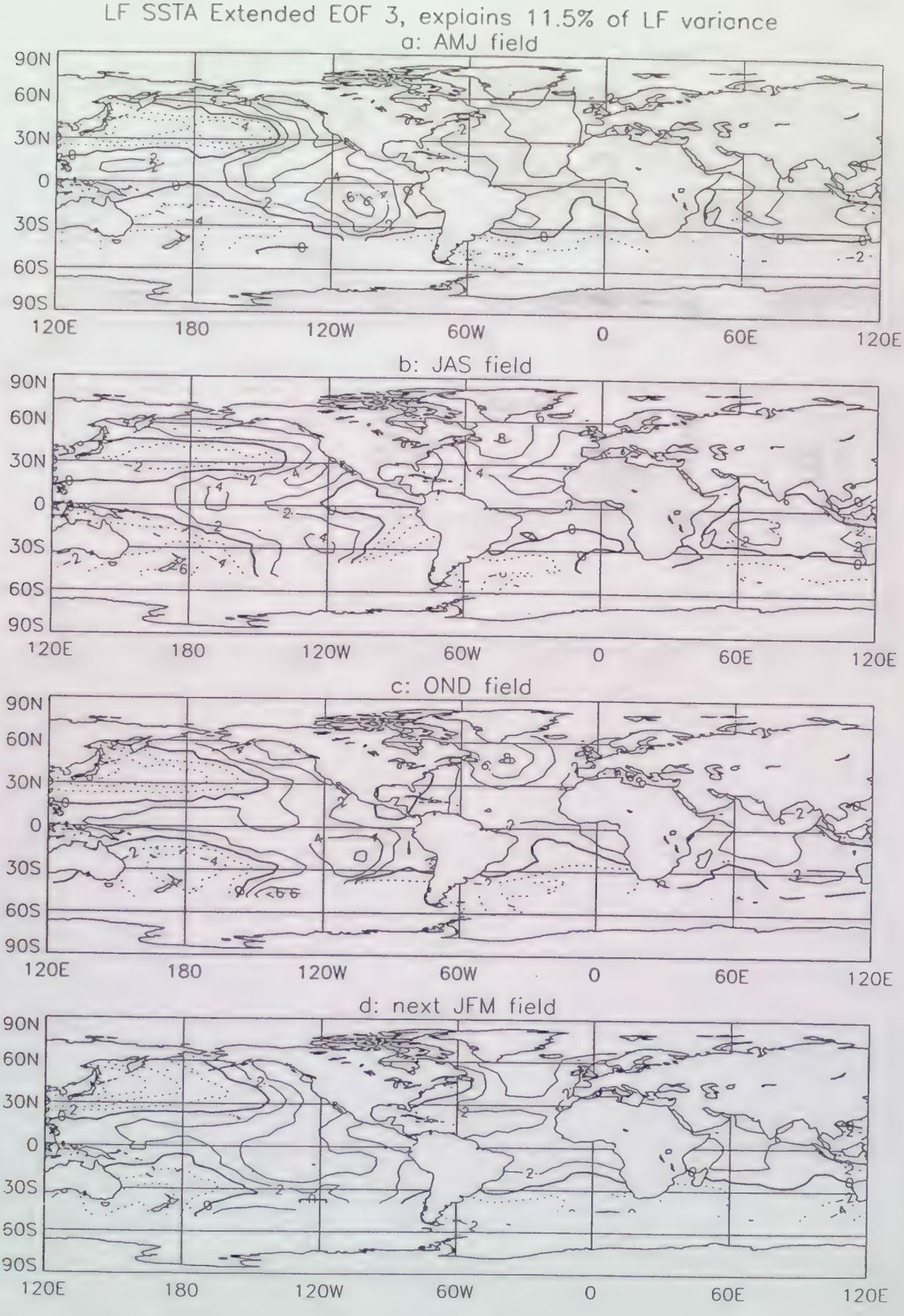
LF SSTA Extended EOF 3, explains 11.5% of LF variance
a: AMJ field
b: JAS field
c: OND field
d: next JFM field
90N
60N
30N
0
30S
60S
90S
120E
180
120W
60W
0
60E
120E

Figure 7

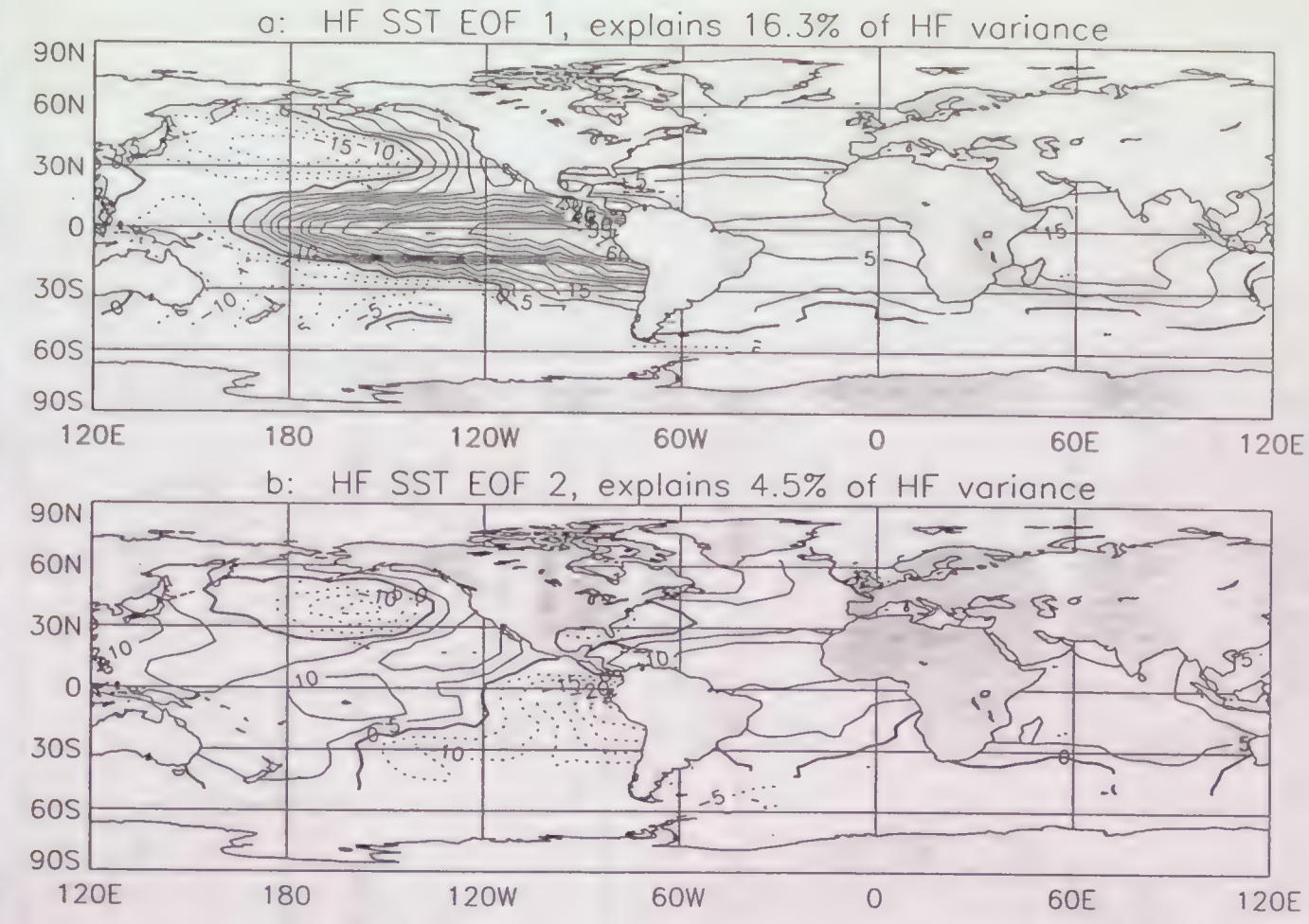
a: HF SST EOF 1, explains 16.3% of HF variance
90N
60N
30N
0
30S
60S
90S
120E
180
120W
60W
0
60E
120E
b: HF SST EOF 2, explains 4.5% of HF variance
90N
60N
30N
0
30S
60S
90S
120E
180
120W
60W
0
60E
120E

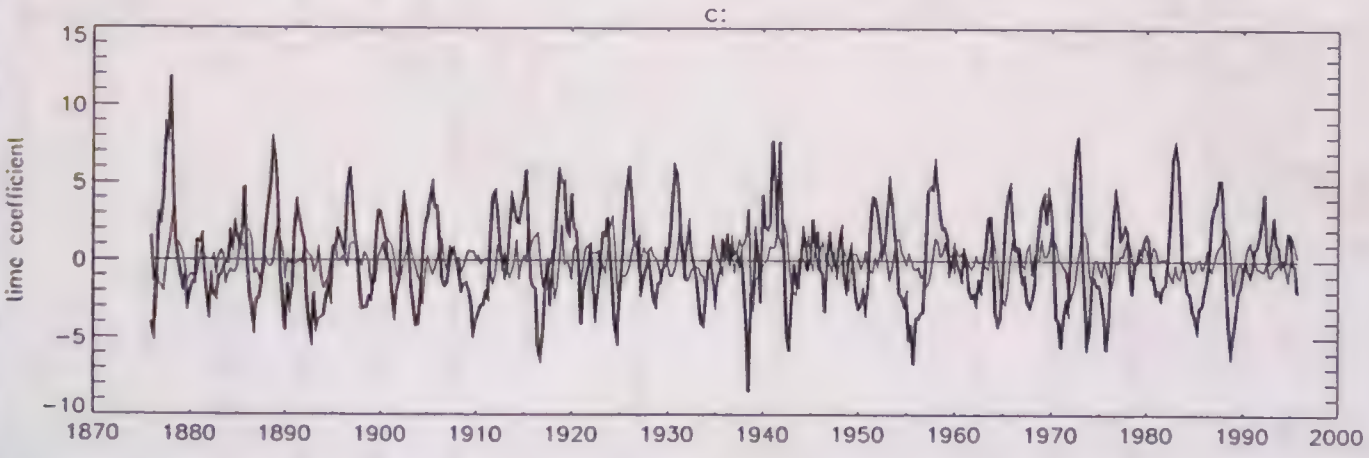
c:
time coefficient
15
10
5
0
−5
−10
1870
1880
1890
1900
1910
1920
1930
1940
1950
1960
1970
1980
1990
2000

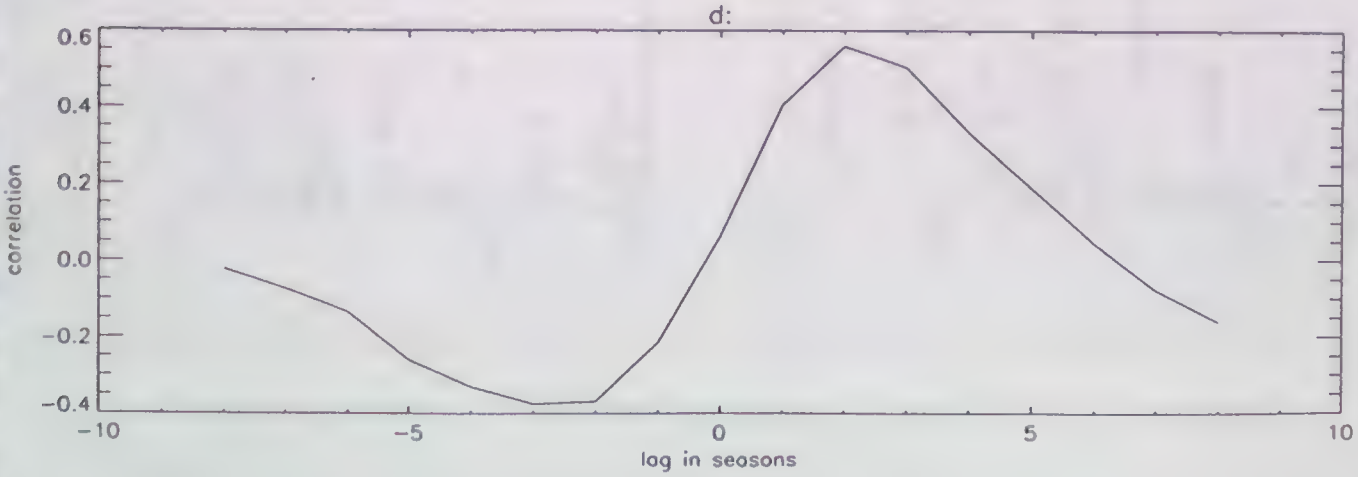
d:
correlation
0.6
0.4
0.2
0.0
−0.2
−0.4
−10
−5
0
5
10
lag in seasons

Figure 8

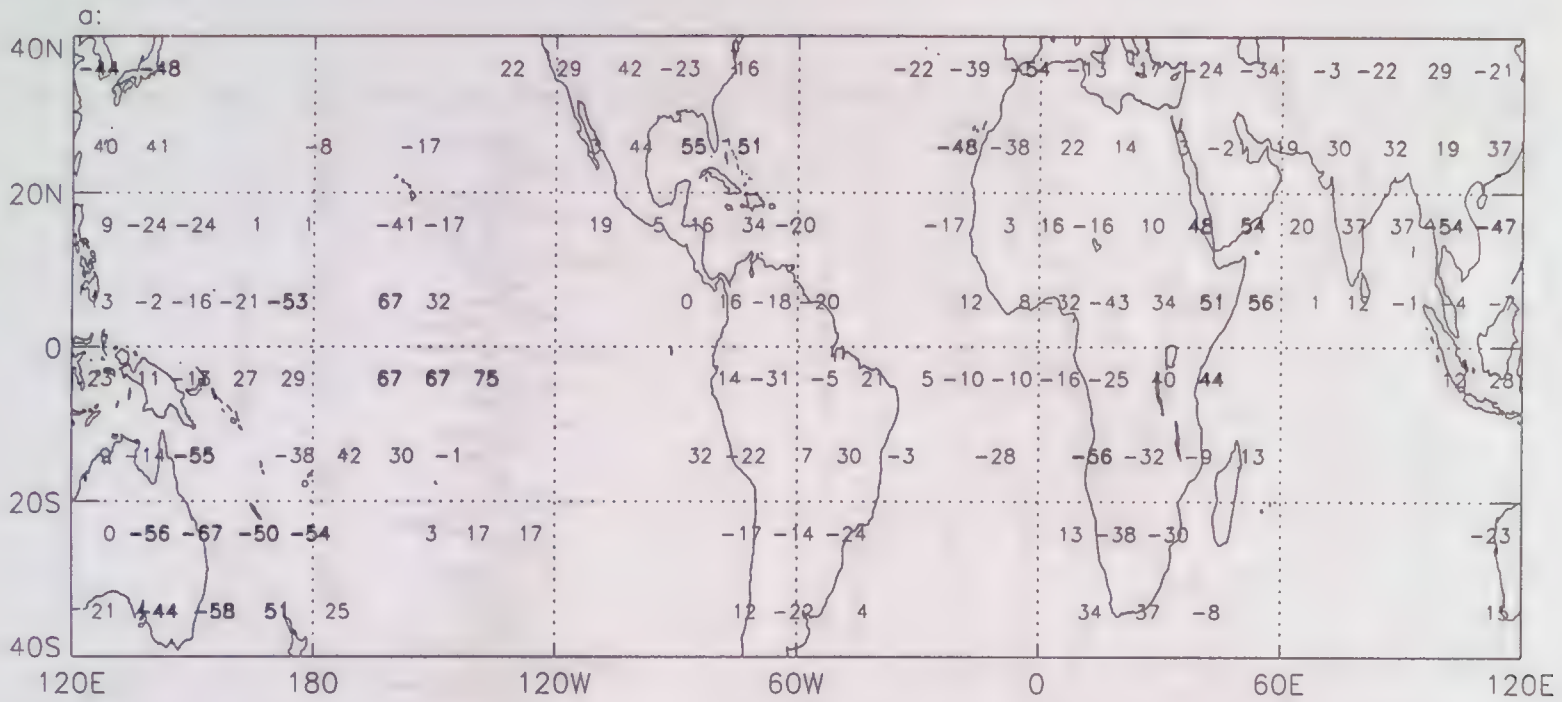
a:
40N
20N
0
20S
40S
120E
180
120W
60W
0
60E
120E

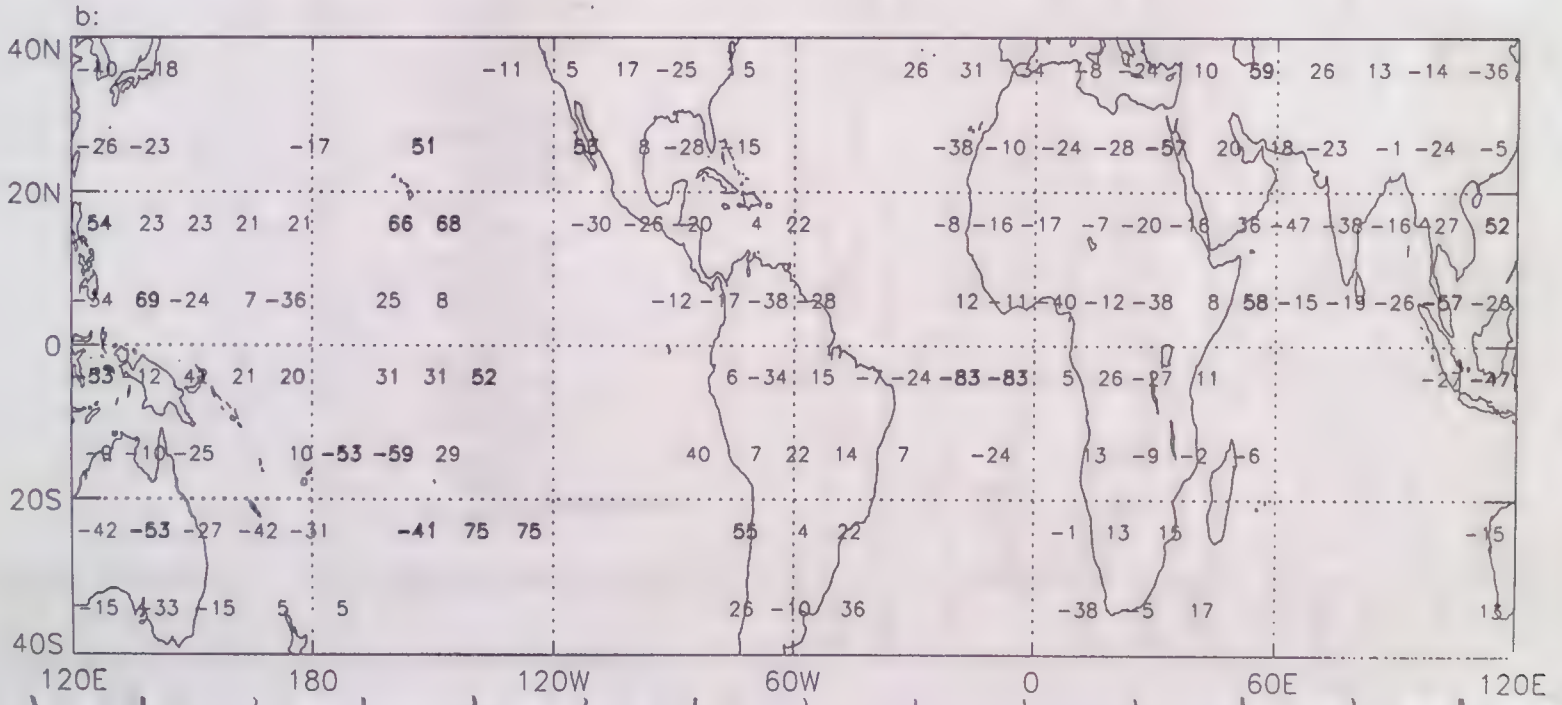
b:
40N
20N
0
20S
40S
120E
180
120W
60W
0
60E
120E

Figure 9

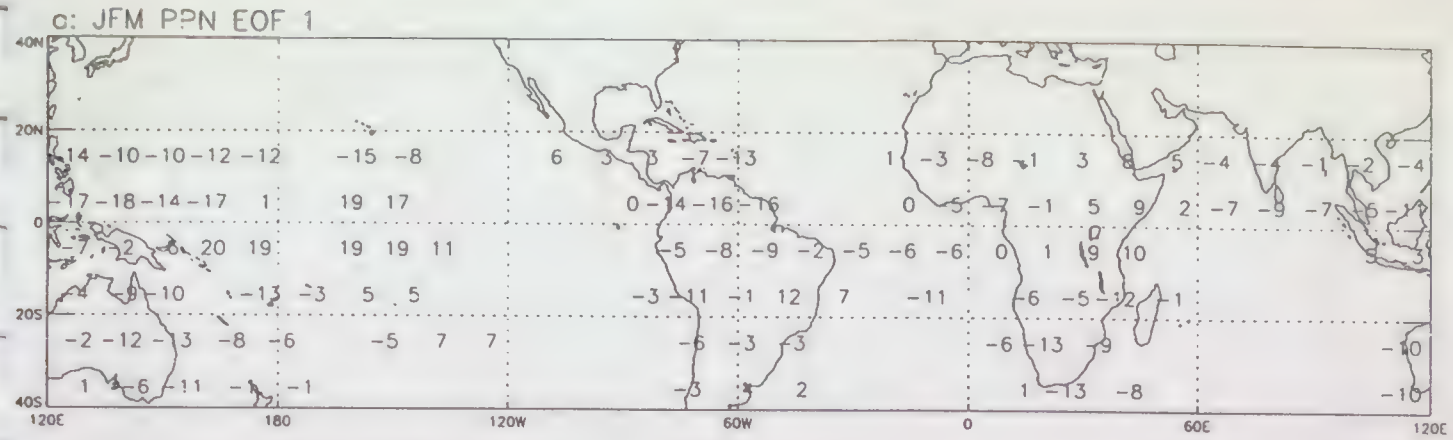
c: JFM PPN EOF 1
40N
20N
0
20S
40S
120E
180
120W
60W
0
60E
120E

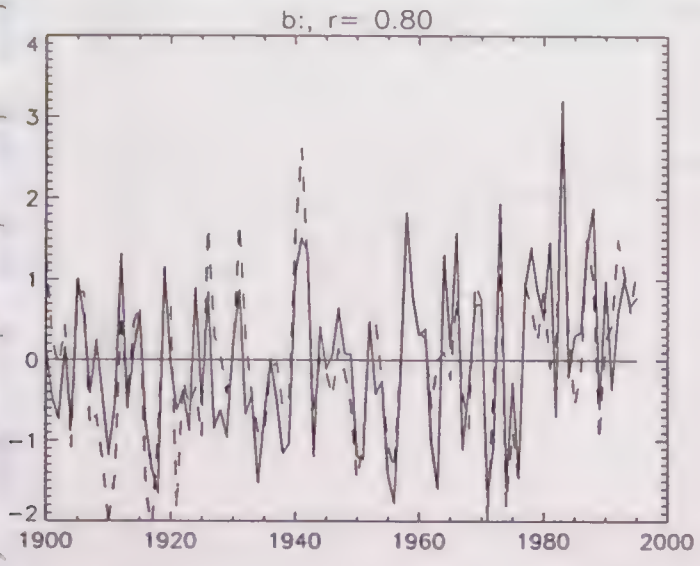
b:, r= 0.80
1900
1920
1940
1960
1980
2000

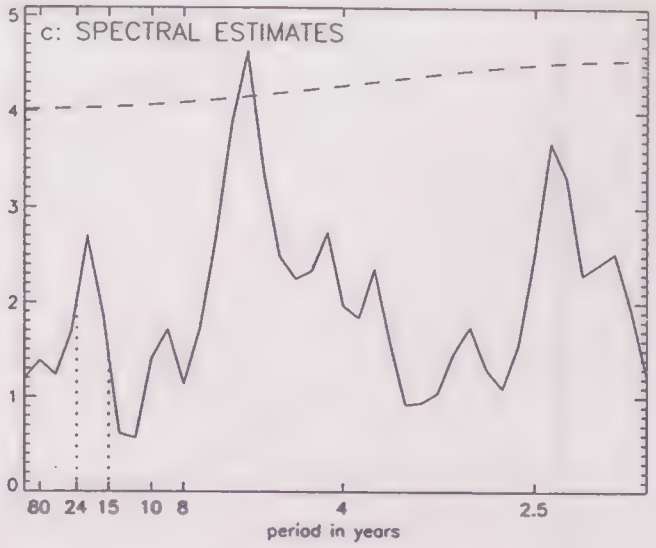
c: SPECTRAL ESTIMATES
80 24 15 10 8
4
2.5
period in years

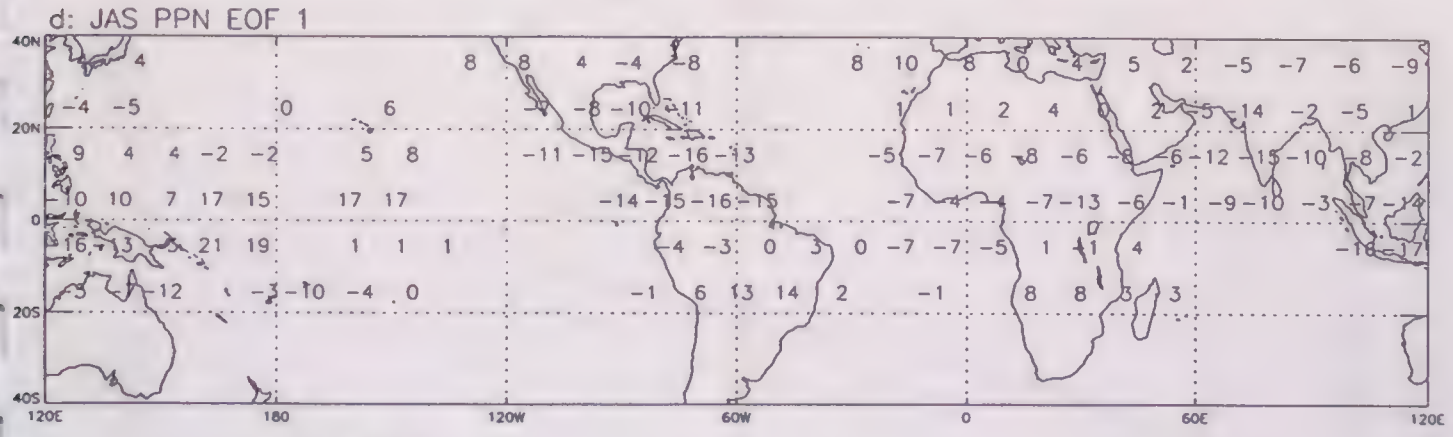
d: JAS PPN EOF 1
40N
20N
0
20S
40S
120E
180
120W
60W
0
60E
120E

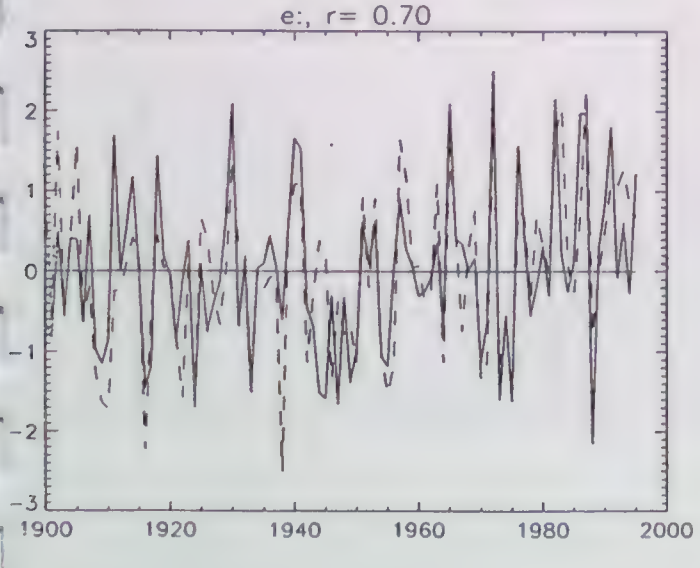
e:, r= 0.70
1900
1920
1940
1960
1980
2000

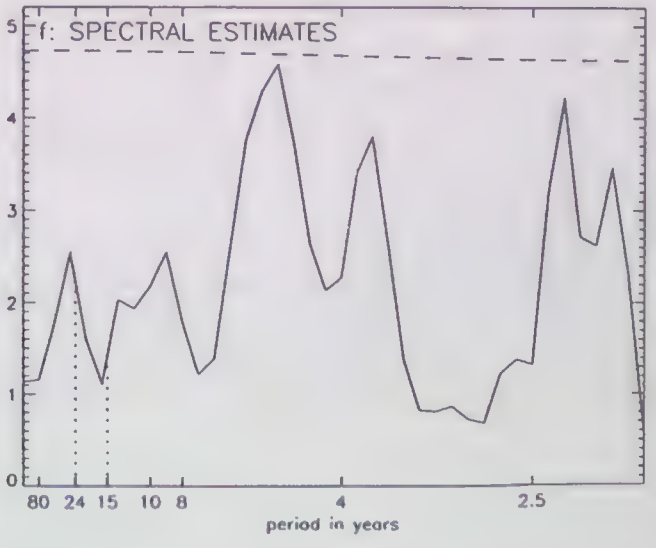
f: SPECTRAL ESTIMATES
80 24 15 10 8
4
2.5
period in years

Figure 10a

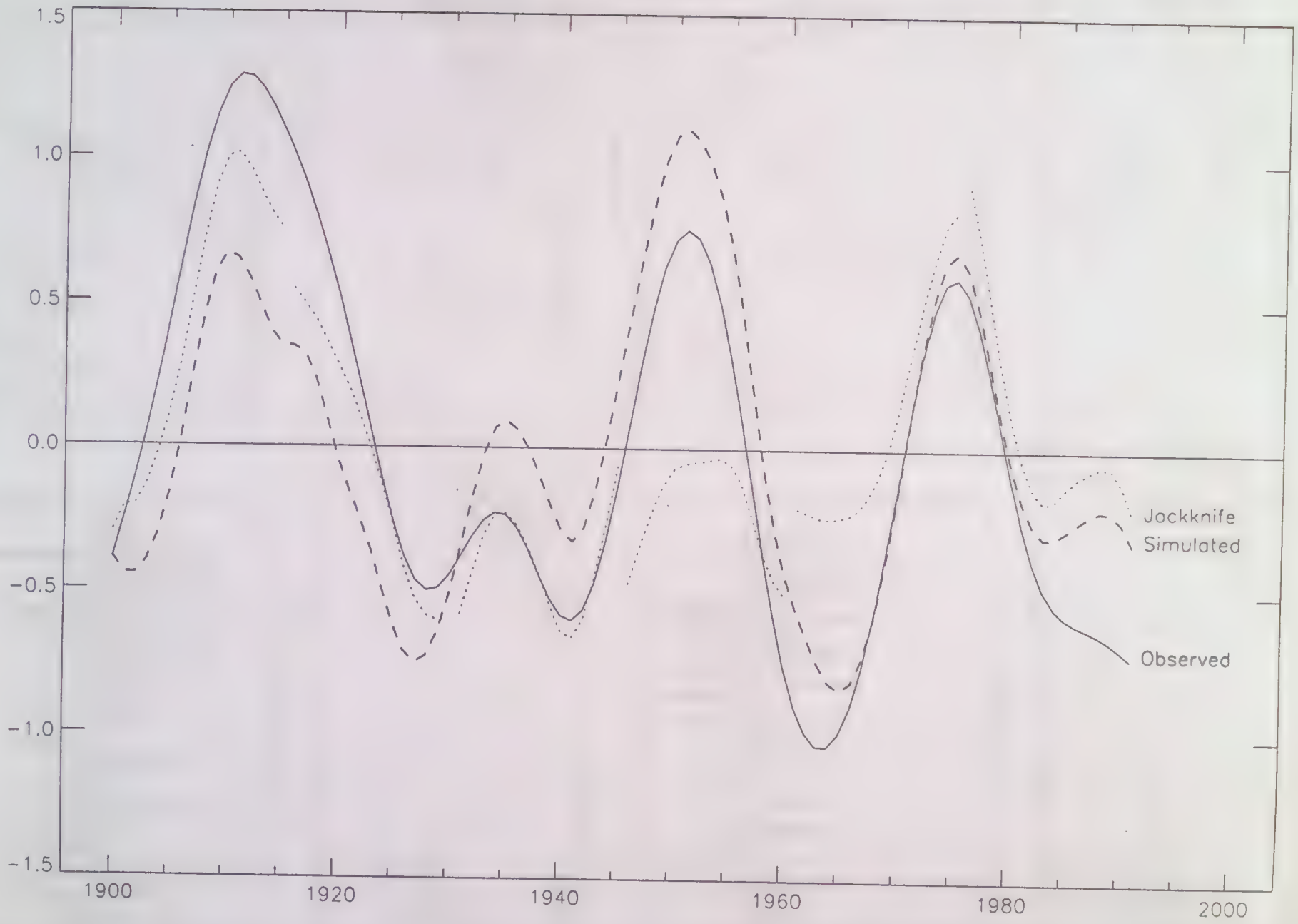
1.5
1.0
0.5
0.0
-0.5
-1.0
-1.5
1900
1920
1940
1960
1980
2000
Jackknife
Simulated
Observed

Figure 10b

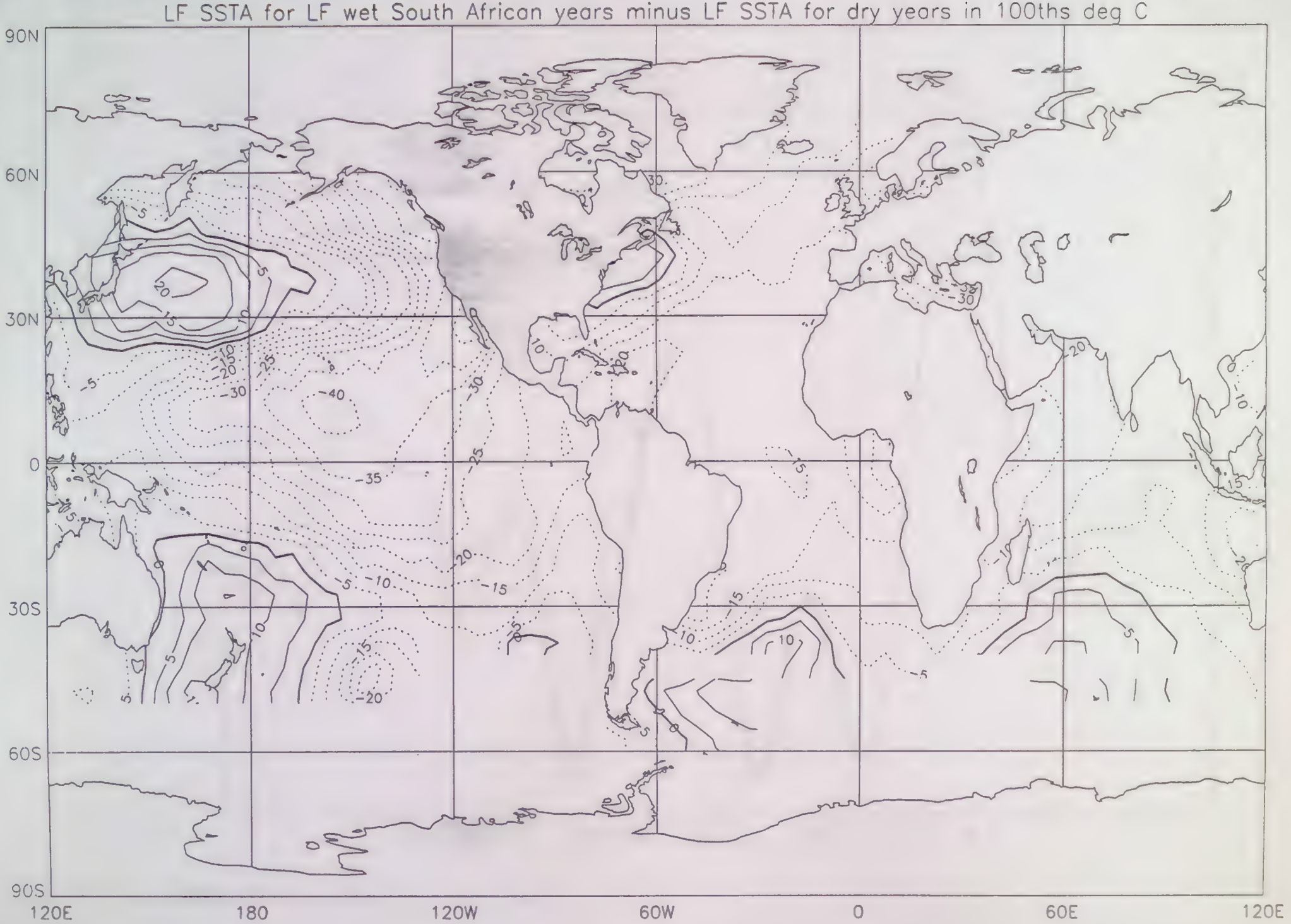
LF SSTA for LF wet South African years minus LF SSTA for dry years in 100ths deg C
90N
60N
30N
0
30S
60S
90S
120E
180
120W
60W
0
60E
120E

Figure A1

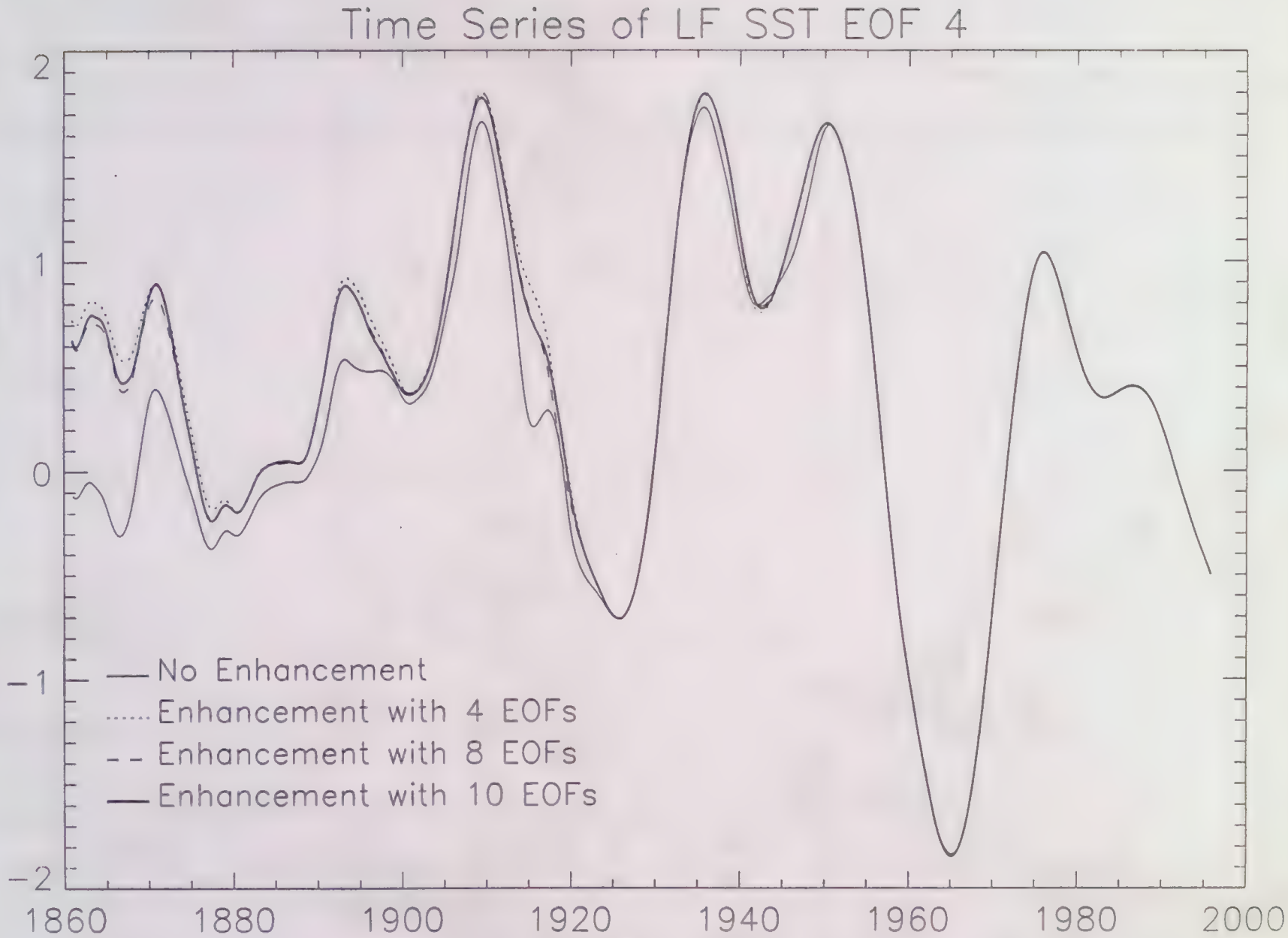
Time Series of LF SST EOF 4
2
1
0
−1
−2
1860
1880
1900
1920
1940
1960
1980
2000
No Enhancement
Enhancement with 4 EOFs
Enhancement with 8 EOFs
Enhancement with 10 EOFs

CLIMATE RESEARCH TECHNICAL NOTES

CRTN 1	Oct 1990	Estimates of the sensitivity of climate to vegetation changes using the Penman-Monteith equation. P R Rowntree
CRTN 2	Oct 1990	An ocean general circulation model of the Indian Ocean for hindcasting studies. D J Carrington
CRTN 3	Oct 1990	Simulation of the tropical diurnal cycle in a climate model. D P Rowell
CRTN 4	Oct 1990	Low frequency variability of the oceans. C K Folland, A Colman, D E Parker and A Bevan
CRTN 5	Dec 1990	A comparison of 11-level General Circulation Model Simulations with observations in the East Sahel. K Maskell
CRTN 6	Dec 1990	Climate Change Prediction. J F B Mitchell and Qing-cun Zeng
CRTN 7	Jan 1991	Deforestation of Amazonia - modelling the effects of albedo change. M F Mylne and P R Rowntree
CRTN 8	Jan 1991	The role of observations in climate prediction and research. D J Carson
CRTN 9	Mar 1991	The greenhouse effect and its likely consequences for climate change. D J Carson
CRTN 10	Apr 1991	Use of wind stresses from operational N.W.P. models to force an O.G.C.M. of the Indian Ocean. D J Carrington
CRTN 11	Jun 1991	A new daily Central England Temperature series, 1772-1991. D E Parker, T P Legg and C K Folland
CRTN 12	Jul 1991	Causes and predictability of Sahel rainfall variability. D P Rowell, C K Folland, K Maskell, J A Owen, M N Ward

CLIMATE RESEARCH TECHNICAL NOTES

CRTN 13	Jul 1991	Modelling changes in climate due to enhanced CO2, the role of atmospheric dynamics, cloud and moisture. C A Senior, J F B Mitchell, H Le Treut and Z-X Li
CRTN 14	Sep 1991	Sea temperature bucket models used to correct historical SST data in the Meteorological Office. C K Folland
CRTN 15	Aug 1991	Modelling climate change, and some potential effects on agriculture in the U.K. P R Rowntree, B A Callander and J Cochrane
CRTN 16	Aug 1991	The Boreal Forests and Climate G Thomas and P R Rowntree
CRTN 17	Aug 1991	Development of a Stratosphere-Troposphere Data Assimilation System. R Swinbank.
CRTN 18	Sep 1991	A study of asynchronous coupling using a simple climate model. M K Davey.
CRTN 19	Sep 1991	The Oceanic Carbon Cycle. N K Taylor
CRTN 20	Nov 1991	Worldwide ocean-atmosphere surface fields in Sahel wet and dry years using provisionally corrected surface wind data. M N Ward
CRTN 21	Dec 1991	Coupled tropical ocean global atmosphere models at the UKMO. M K Davey, C Gordon, S Ineson and S Lawrence
CRTN 22	Dec 1991	Empirical parameterisation of tropical ocean-atmosphere coupling. M Allen, M K Davey, D L T Anderson and P D Killworth
CRTN 23	Feb 1992	The temporal evolution of Equatorial Currents in the Indian Ocean D L T Anderson, D J Carrington, R A Corry and C Gordon
CRTN 24	Feb 1992	Stratospheric analyses provided by the U.K. Meteorological Office M J Bailey, A O'Neill and V D Pope

CLIMATE RESEARCH TECHNICAL NOTES

CRTN 25	Feb 1992	Modelling interannual variability in the Indian Ocean using momentum fluxes from the UKMO and ECMWF operational weather analyses. D L T Anderson and D J Carrington
CRTN 26	Mar 1992	A GCM simulation of the impact of Amazonian deforestation on climate using an improved canopy representation J Lean and P R Rowntree
CRTN 27	Mar 1992	The parameterization of rainfall interception in GCMs A J Dolman and D Gregory
CRTN 28	Jun 1992	Development of worldwide marine data eigenvectors since 1985 A W Colman
CRTN 29	Jun 1992	A tropical ocean model with reduced physics M K Davey
CRTN 30	Jun 1992	International Temperature Workshop, Boulder, Colorado, USA, 16 January 1992 Edited by D E Parker
CRTN 31	Jul 1992	Simulation of clear-sky outgoing longwave radiation over the oceans using operational analyses A Slingo and M J Webb
CRTN 32	Sep 1992	A prediction of the transient response of climate J M Murphy
CRTN 33	Nov 1992	LEPS scores for assessing climate model simulations and long-range forecasts. C K Folland
CRTN 34	Jan 1993	Stratospheric Data Assimilation System Guide Editer: R Swinbank
CRTN 35	Mar 1993	A Stratosphere-Troposphere Data Assimilation System R Swinbank and A O'Neill
CRTN 36	Mar 1993	Validation of hydrological schemes for climate models against catchment data. P R Rowntree and J Lean

CLIMATE RESEARCH TECHNICAL NOTES

CRTN 37	Apr 1993	Modelling of palaeoclimates: Examples from the recent past J F B Mitchell
CRTN 38	May 1993	A simulation of seasonality in ENSO forecast skill M K Davey, D L T Anderson and S Lawrence
CRTN 39	Jul 1993	ENSO Prediction experiments using a simple ocean-atmosphere model D-H Wu, D L T Anderson and M K Davey
CRTN 40	Sep 1993	Diagnosis of dynamic sea-surface and sea-level changes from the Cox ocean model J M Gregory
CRTN 41	Sep 1993	Seasonal variations of the clear-sky greenhouse effect: the role of changes in atmospheric temperatures and humidities M J Webb, A Slingo and G L Stephens
CRTN 42	Nov 1993	Sea-level changes under increasing atmospheric CO_2 in a transient coupled ocean-atmosphere GCM experiment. J M Gregory
CRTN 43	Dec 1993	Global and regional patterns of climate change: recent predictions for the Arctic P R Rowntree
CRTN 44	Feb 1994	The effect of changing horizontal diffusion in the atmospheric version of the unified climate model C D Hall and R A Stratton
CRTN 45	Mar 1994	Simulation of El-Niño/Southern Oscillation like variability in a global AOGCM and its response to CO_2 increase. S F B Tett
CRTN 46	Apr 1994	Global data required for monitoring climate change. D E Parker and C K Folland
CRTN 47	May 1994	Seasonal uptake of anthropogenic CO_2 in an ocean general circulation model. N K Taylor

CLIMATE RESEARCH TECHNICAL NOTES

CRTN 48	Jun 1994	A tropic-wide oscillation of boreal summer rainfall and patterns of sea-surface temperature. M N Ward, K Maskell, C K Folland, D P Rowell and R Washington
CRTN 49	Jun 1994	Simulation of the tropical Pacific using a simplified ocean model M A Balmaseda, D L T Anderson and M K Davey
CRTN 50	Sep 1994	Simulation of global mean temperature using a box-diffusion climate model P R Rowntree
CRTN 51	Sep 1994	Seasonal dependence of ENSO prediction skill M A Balmaseda, M K Davey and D L T Anderson
CRTN 52	Nov 1994	Simulation of the Indian Monsoon and Tropical Intraseasonal Variability by a General Circulation Model P M Inness and D Gregory
CRTN 53	Mar 1995	A comparison of modelled surface fluxes with climatological estimates. C Gordon and D K Wright
CRTN 54	Mar 1995	The representation of moist convection in atmospheric models. D Gregory
CRTN 55	Mar 1995	A consistent treatment of the evaporation of rain and snow for use in large-scale models D Gregory
CRTN 56	Apr 1995	Workshop on simulations of the Climate of the Twentieth Century using GISST, 28-30 November 1994, Hadley Centre, Bracknell, UK Edited by C K Folland and D P Rowell
CRTN 57	May 1995	Enhanced shortwave cloud radiative forcing due to anthropogenic aerosols. S E Swartz and A Slingo
CRTN 58	May 1995	The simulation of the tropical oceans in models of different horizontal resolution. C Gordon, D K Wright and C M Roberts
CRTN 59	Sep 1995	The water budget of middle latitude continental regions - a modelling and observational study P R Rowntree
CRTN 60	Sep 1995	Intraseasonal variability of the Indian summer monsoon simulated by the Hadley Centre climate model K Ashok, D Gregory and P M Inness

CLIMATE RESEARCH TECHNICAL NOTES

CRTN 61	Sep 1995	Climate simulations with the Unified Model: AMIP runs C D Hall, R A Stratton and M L Gallani
CRTN 62	Nov 1995	Validation of surface parameters over the oceans in climate simulations with the unified model. C D Hall
CRTN 63	Dec 1995	The GISST2.2 sea surface temperature and sea-ice climatology D E Parker, M Jackson and E B Horton
CRTN 64	Dec 1995	Parametrization of momentum transport by convection. II: Tests in single column and general circulation models. D Gregory, R Kershaw and P M Inness
CRTN 65	Jan 1996	Understanding the sensitivity of a GCM simulation of Amazonian deforestation to the specification of vegetation and soil characteristics. J Lean and P R Rowntree
CRTN 66	Jan 1996	On the efficient calculation of infra-red fluxes and cooling rates using the two-stream equations. J M Edwards
CRTN 67	Jan 1996	The second Hadley Centre coupled ocean-atmosphere GCM: Model description, spinup and validation. TC Johns,RE Carnell,JF Crossley,JM Gregory, JFB Mitchell,CA Senior,SFB Tett and RA Wood
CRTN 68	Feb 1996	The sensitivity of climate simulations to the specification of mixed phase clouds D Gregory and D Morris
CRTN 69	Apr 1996	Using an ensemble of Multi-Decadal GCM simulations ro assess potential seasonal predictability D P Rowell
CRTN 70	May 1996	North Atlantic and European Seasonal Predictability using an Ensemble of Multi-Decadal AGCM Simulations J R Davies, D P Rowell and C K Folland
CRTN 71	Jun 1996	A description of the Second Hadley Centre Coupled Model (HADCM2) T C Johns
CRTN 72	Jul 1996	Palaeoclimate Modelling Intercomparison: UKMO GCM simulations for 6kBP and 21kBP C D Hewitt and J F B Mitchell

CLIMATE RESEARCH TECHNICAL NOTES

CRTN 73	Aug 1996	ENSO responses and low frequency weather variability in the North Pacific/American sector 1949-93 A C Renshaw, D P Rowell and C K Folland
CRTN 74	Sep 1996	Version 2.2 of the Global sea-Ice and Sea Surface Temperature data set, 1903-1994 N A Rayner, E B Horton, D E Parker, C K Folland and R B Hackett
CRTN 75	Sep 1996	A new gravity wave drag scheme incorporating anisotropic orography and low level wave breaking : Impact upon the climate of the UK Met Office Unified Model D Gregory, G J Shutts and J R Mitchell
CRTN 76	Nov 1996	Middle atmosphere variability in the UKMO Unified Model R Swinbank, W Lahoz, C Douglas, A Heaps, R Brugge, W Norton, A O'Neill, D Podd
CRTN 77	Dec 1996	A high resolution AMIP run using the Hadley Centre model HadAM2b R A Stratton
CRTN 78	Jan 1997	The climate response to CO_2 of the Hadley Centre coupled AOGCM with and without flux adjustment J M Gregory and J F B Mitchell
CRTN 79	May 1997	Development of the Global Mean Sea Level Pressure Data Set GMSLP2 T A Basnett and D E Parker
CRTN 80	Jun 1997	Seasonal Forecasting D J Carson
CRTN 81	Feb 1998	Large scale modes of ocean surface temperature since the late nineteenth century C K Folland, D E Parker, A W Colman and R Washington